THERMAL PERFORMANCE OF GRAPHENE COATING ON COPPER
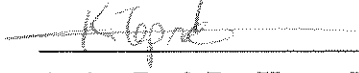
A Thesis Submitted to
the Graduate School of Engineering and Sciences of
İzmir Institute of Technology
in Partial Fulfillment of the Requirements for the Degree of

MASTER OF SCIENCE

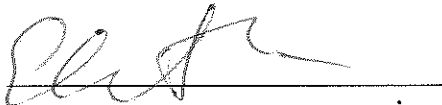in Energy Engineering

by
Gizem ERSAVAŞ

July 2019
İZMİR

We approve the thesis of **Gizem ERSAVAŞ**

Examining Committee Members:

Assist. Prof. Dr. Kasım TOPRAK
Department of Mechanical Engineering
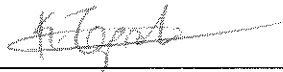İzmir Institute of Technology

Assoc. Prof. Dr. Erdal ÇETKİN
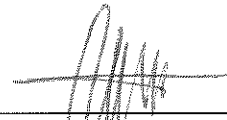Department of Mechanical Engineering
İzmir Institute of Technology

Assist. Prof. Dr. Ebubekir ATAN
Department of Mechanical Engineering
İzmir Kâtip Çelebi University

17 July 2019

Assist. Prof. Dr. Kasım TOPRAK
Supervisor
Department of Mechanical Engineering
İzmir Institute of Technology

Assoc. Prof. Dr. Cem ÇELEBİ
Co-supervisor
Department of Physics
İzmir Institute of Technology

Prof. Dr. Gülden Gökçen AKKURT
Head of the Department of
Energy Engineering

Prof. Dr. Aysun SOFUOĞLU
Dean of the Graduate School of
Engineering and Sciences

ACKNOWLEDGMENTS

ABSTRACT

THERMAL PERFORMANCE OF GRAPHENE COATING ON COPPER

Over heat is always a problem for electronic devices because the locally generated heat cannot be transferred appropriately to the corresponding heat sink fast enough. This situation leads to affect materials' structures, mechanical properties and conductivities badly. In order to avoid this problem, high thermal conductivity materials are used to dissipate the heat quickly.

Thanks to the development of technology, the size of the electronic devices is reduced day by day. This also shrinks the size of the interconnect components. So this situation leads to researchers to investigate nano-sized interconnect components and copper, which is a widely used material, is one of them. Copper is one of the preferred metals for electronic devices because of high thermal conductivity, easy processability, and high use in daily life and industry. For example, copper components, which is used in electronic, are getting so thin and must carry so much current. And that causes to increase friction. Thus heat is occurred. Consequently, cooling problems have arisen. And if the material's cooling problem won't be solved then the material can be damaged. It is thought that to overcome this problem, coating with a high thermal conductivity material such as graphene, the thermal conductivity can be improved. In this study, thermal performance of graphene-coated copper were investigated numerically and experimentally.

This study consist of two main sections. The first part, MD simulation code was created using C++ programming language to investigate thermal conductivity of copper, different number of graphene layers and these graphene layers were coated on copper in different length, width, height and temperature. In the second part, the thermal performance of pure copper, annealed copper, a layer of graphene-coated copper, and multi-layer graphene-coated copper was studied by the experimental setup at three different temperatures and volume flow rates.

ÖZET

GRAFEN KAPLI BAKIRIN TERMAL PERFORMANSI

Yüksek ısı elektronik cihazlar için her zaman sorun oluşturmaktadır. Bunun nedeni, üretilen ısının uygun ve hızlı bir şekilde soğutucu tarafından atılamamısıdır. Yüksek ısının atılamaması malzemenin yapısını, mekanik özelliklerini, ısı ve elektrik iletimini kötü bir şekilde etkiler. Bu durumu önlemek için yüksek termal iletkenliğe sahip malzemeler kullanılarak, ısının hızlı bir şekilde atılması sağlanır.

Teknolojideki gelişmeler sayesinde, elektronik cihazların boyutları gün geçtikçe azalmaktadır. Bu durum, elektronik cihazların içerisindeki bağlantı elemanlarının da boyutlarının küçülmesine neden olmaktadır. Bunun sonucunda, bazı araştırmacılar nanoboyutlardaki baglantı elemanlarını incelemeye ve bu elemanların performansını iyileştirmeye yonelmiştir.Yaygın olarak kullanılan bir malzeme olan bakır da bunlardan biridir. Bakır yüksek termal iletkenlikleri, kolay işlenebilirlikleri, günlük hayatta ve sanayide çok fazla kullanılmaları yüzünden elektronik donanımlar için tercih edilen metallerdendir. Örnek vermek gerekirse elektronikte kullanılan bakır parçaların boyutları gün geçtikçe küçülmektedir ve çok fazla akıma maruz kalmaktadır. Bu durum nakır nanoteller içindeki direnci arttırır ve ısı oluşmasına neden olur. Bu da nanotellerde soğutma problemini ortaya çıkarmıştır ve eğer kullanılan malzemedeki soğutma probelemi çözülmez ise malzeme zarar görebilir. Bu problemlemin üstesinden gelmek için kullanılan malzemenin üzeri grafen gibi yüksek termal iletkenliğe sahip bir malzeme ile kaplanarak thermal iletkenliğinin iyilileştirilebileceği düşünülmektedir. Bu çalışma, grafen kaplı bakırın termal özelliklerini numerik ve deneysel olarak incelenmiştir.

İki ana bölümden oluşan bu çalışmanın ilk kısmında C++ programlama dili kullanılarak bakırın, farklı sayıdaki grafen katmanının ve bu grafen katmanlarının bakır üzerine kaplandığı modelleri oluşturuldu ve moleküler dinamik simülasyon yöntemi kullanılarak thermal iletkenliğin değişimi farklı uzunluk, genişlik, yükseklik ve sıcaklıkta incelenmiştir. İkinci kısımda ise, saf bakırın, tavlanmış bakırın, bir katman grafen kaplamalı bakırın ve çok katman grafen kaplmalı bakırın termal performansı bir deney düzeneği kurularak farklı sıcaklık ve debide incelenmiştir.

TABLE OF CONTENTS

LIST OF FIGURES

LIST OF TABLES

CHAPTER 1

INTRODUCTION

The developments in technology and science enable shrinking the size of electronic devices to micro- and nano- sizes. As the sizes reduce, the heat dissipation problem has become a very important issue. If the locally generated heat cannot be removed from the material or transferred fast enough to the corresponding heatsink, it may cause overheating problem that is always a crucial problem for all area of thermal applications. Thus, many studies have been done in the literature to solve this problem since overheating affects material structures and mechanical and physical properties badly.

In the field of nanoelectronics among the electronic components, one of the most widely used materials as a heat sink is copper (Hong et al., 2015). Therefore, it is important to enhance copper's thermal conductivity for dissipating heat rapidly and protect the material from the high temperatures. At this point, using high thermal conductivity materials helps to dissipate the heat quickly (Balandin et al., 2008; Guo et al., 2009).
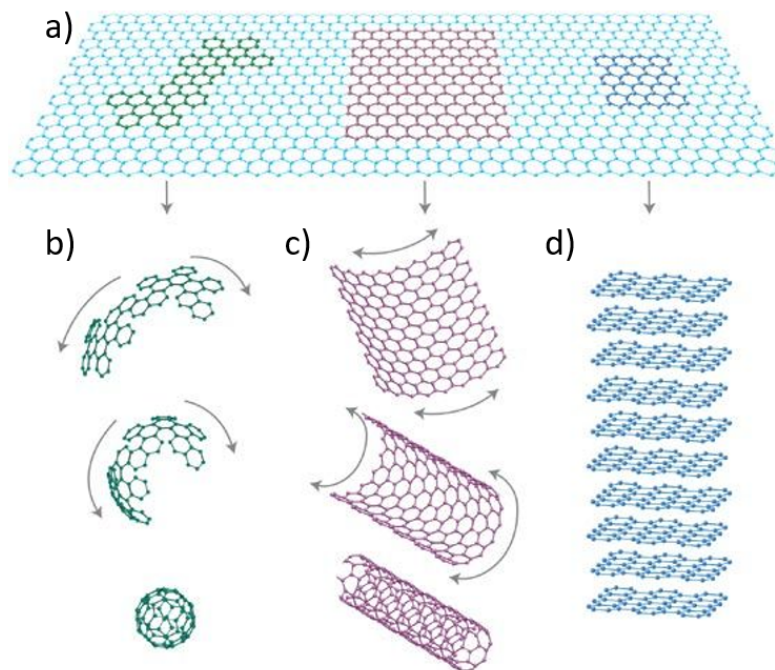
Figure 1.1. Schematic structure of carbon materials with different dimensions: a) 2-D graphene b) fullerene, c) carbon nanotube, d) graphite. (Source: Novoselov and Geim, 2007)

In 2004, new carbon-based material of graphene was discovered. It is obtained by extracting layer from graphite and that single layers are called graphene layers (Novoselov et al., 2004). This discovery has dazzled researchers to study graphene widely. Graphene is one of the basic structural of among carbon-based materials including graphite, carbon nanotubes and fullerenes which is shown in Figure 1.1.

Graphene has two-dimensional, one atom thick layer and sp^2 bonded in a hexagonal lattice (Balandin et al., 2008) which is illustrates in Figure 1.2. The carbon atoms are connected by strong covalent bonds and the bond lenght is 0.142 nm and the bond angle is 120 degree. These properties give graphene a unique properties. Graphene is the lightest, strongest, transparent, flexible, and a conductive material which is known (Balandin et al., 2008; Lee et al., 2008; Mortazavi et al., 2012; Mortazavi and Ahzi, 2012).
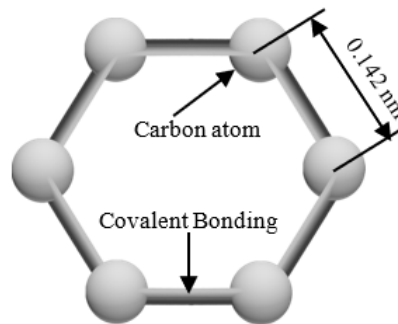
Figure 1.2. Graphene lattice structure.

Numerous studies have been done on graphene applications to help improve the performance and efficiency of the current material. Researchers found that graphene provides a protective coating against corrosion (Usha Kiran et al., 2017; Hu et al., 2014). Another study showed that graphene-composite materials help to make flexible copper nano-wires for electronic components to decrease the high power density on them (Mehta et al., 2015). Also in 2014, LG produced a flexible touchscreen with the help of graphene. Furthermore, a heatable smart window is made from the graphene-based composite material for the cold days to protect car glass from icing by using marvelous thermal performance of graphene (Kang et al., 2011).

Among all of these properties, this study interest improving the thermal conductivity of copper using the high thermally conductive material and graphene is known as the highest thermal conductivity compared to other carbon-based materials (Balandin et al., 2008; Balandin, 2011). Balandin et al. (2008) reported first experimental study of the thermal conductivity on single layer graphene using a Raman spectroscopy and they found its

thermal conductivity about 4840 W/mK to 5300 W/mK.

Graphene structure is called zigzag and armchair according to the direction of heat in it which is demonstrated in Figure 1.3. Heat transport in graphene dominated by phonons and affected by the length of phonon mean free path (PMFP) that is about ~ 600 nm near room temperature (Hsieh et al., 2017). Thus, it gives graphene unique thermal properties. The thermal conductivity of graphene calculated according to the Boltzmann transport equation and researchers found that is about ~ 3000 W/mK at near room temperature (Lee et al., 2013).
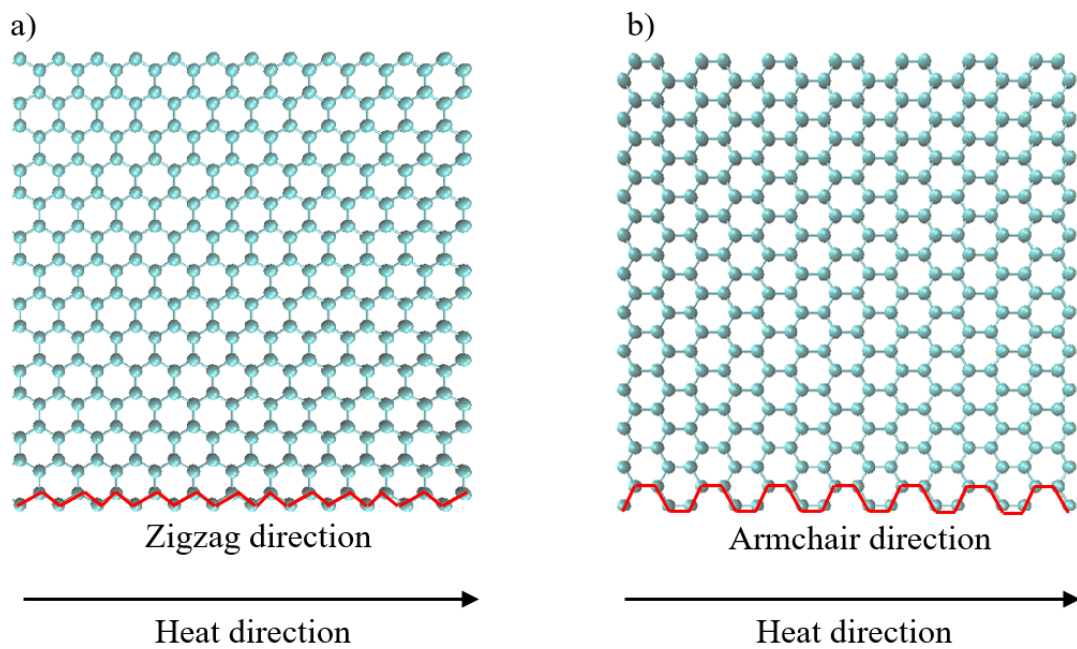
Figure 1.3. Heat direction in graphene, a) Zigzag direction, b) Armchair direction.

As a result of that graphene-coated copper and calculate thermal conductivity of graphene-coated materials become a hot topic. Thus, firstly, researchers have studied graphene synthesis on copper to show the applicability (Hsieh et al., 2017; Lee et al., 2013; Li et al., 2009; Gao et al., 2013). After the graphene synthesis is obtained as a single layer/multilayer or coated on copper, some works have done to calculate thermal conductivity experimentally and numerically.

In this study, our motivation is calculating thermal conductivity of different concepts of graphene coated copper materials by using a molecular dynamics simulation method and comparing the simulations results with real experiments.

1.1. Literature Review

Experimental studies can provide direct measurements of thermal properties of graphene-metal systems, but they have high experimental costs and limited capability of micro/nanoscale temperature probing and thermal detection. On the other hand, numerical simulations are a very efficient way in terms of time and experimental cost. Also, numerical simulations are described the fundamental interactions which couldn't be seen in macro sizes well. In this section, experimental and numerical method can be described on the graphene coated copper.

1.1.1. Experimental Investigation of Graphene Coated Copper

As can be mentioned before, copper is one of the most widely used materials in the electronics industry because of high thermal conductivity. As an earlier study Ashcroft and Mermin (1976) found coppers thermal conductivity about 385 W/mK. With the discovery of graphene, coating it on the copper has become an important topic to improve copper thermal performance.

There are several methods for the fabrication of graphene and the thermal chemical vapor deposition (CVD) method is one of them. Numerous researchers have used this method to fabricate graphene on copper (Goli et al., 2014; Li et al., 2009; Yin et al., 2017; Kang et al., 2013; Wejrzanowski et al., 2016).
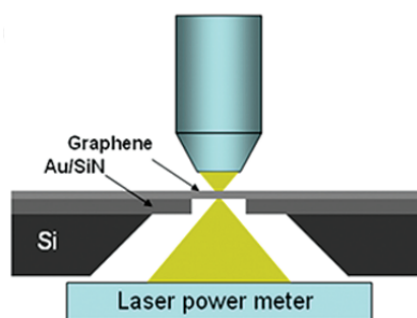
Figure 1.4. Representation of Laser Heating method.
(Source: Cai et al., 2010)

Cai et al. (2010) investigated thermal conductivity of suspended graphene and supported graphene with copper by CVD. They found the thermal conductivity decreases with the temperature increases. As a result, they measured by the laser heating method

which is demonstrated in Figure 1.4. The thermal conductivity of the suspended graphene exceeds 2500 W/mK near the room temperature and 1400 W/mK at 500 K. Also, they obtain the thermal conductivity of the supported graphene smaller than the suspended graphene at the room-temperature.

As a different method Mehta et al. (2015) used plasma enhanced CVD method to coat graphene on copper nano-wire all surfaces. Also, they investigated the electrical and thermal conductivity of graphene coated copper nanowires using Joule heating experiments. They found the thermal and electrical performance of graphene coated copper wires are improve. Also, they reported that size scaling is an important factor. Further, it is found graphene coated copper nanowires has faster data transfer and lower peak temperature compared to the uncoated ones. As it can be seen from Figure 1.5, uncoated copper wires structures get damaged, when the same amount of current gives the nanowires.
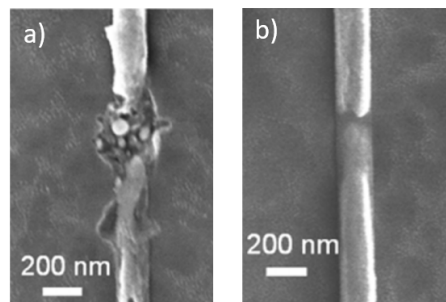
Figure 1.5. Breakdown characteristic of a) un-coated copper wire, b) coated copper wire with the same amount of current. (Source: Mehta et al., 2015)

Hsieh et al. (2017) studied in-plane and through plane thermal conductivity of graphene, carbon nanotube and coated with copper. They synthesized graphene using catalytic chemical vapor deposition and designed two experimental set-ups for analyzing the samples thermal conductivities as in-plane and through-plane direction. Their results show that, the graphene coated samples thermal conductivity is higher than the carbon nanotube coated ones. Further, the in-plane thermal conductivity gives a higher value than through-plane thermal conductivity due to the movements of phonons of the heat transport mechanism in the graphene structure.

Goli et al. (2014) used CVD method to fabricate single-layer and multi-layer graphene on both sides of copper films. They experimentally demonstrated that thermal conductivity of graphene-Cu-graphene heterogeneous film was increased compared to the pure copper and annealed copper by using using laser flash method which is demonstrated in Figure 1.6. They found the thermal conductivity of copper, annealed copper, SLG-Cu

and MLG-Cu system has 25 micrometer thickness 313 W/mK, 337 W/mK, 363 W/mK, and 376 W/mK respectively.
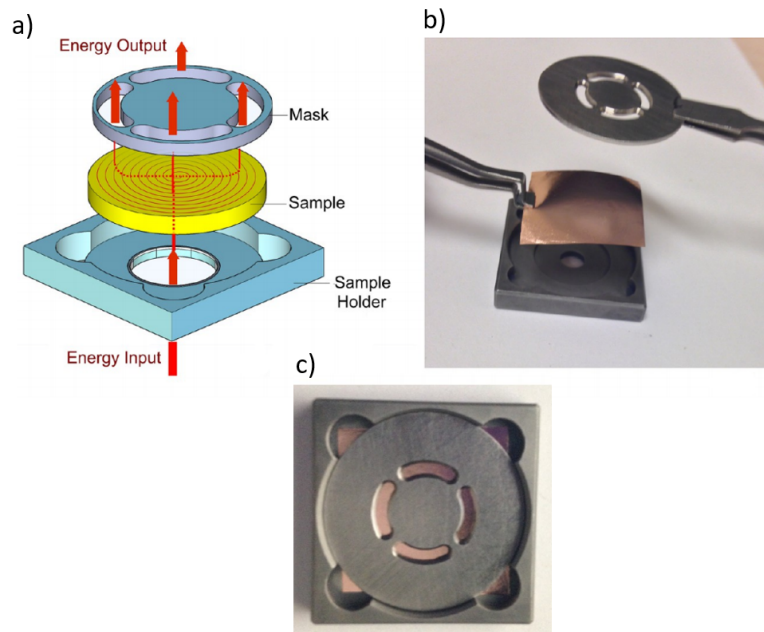
Figure 1.6. Representation of Laser Flash method a) Schematic model of the experimental set-up, b) Placing graphene coated copper on the sample holder, c) View of the sample in the sample holder. (Source: Goli et al., 2014)

Shenoy (2012) designed an experimental set-up for cooling of the heat sink using microchannels and studied carbon nanotubes embedded in water for testing it at different flow rates. He found that heat removal performance of carbon nanotubes embedded water is better than the normal water. In addition to that, it was found high volume flow rates cause higher heat flux which means higher heat transfer.

Salihoglu et al. (2018) worked on thermal camouflage of graphene-based material. They synthesized multilayer graphene using CVD method then transferred to the gold electrodes which locate on a hot object. They used real-time electrical control for investigating the thermal emission over it. Finally, they demonstrated that thermal camouflage system based on graphene that could hide hot surfaces as cold and cold surfaces as hot using graphene electrodes controlled by electrically.

Kang et al. (2013) studied the effects of multilayer graphene capping on Cu interconnect.They used CVD Method to growth graphene on Ni and then transferred to the Cu.They demonstrated that the current density on the Cu interconnect improved by 18% and resistance is reduced by 2-7% with graphene capping. This provides longer lifetime and better conductivity to the copper interconnect. Figure 1.7 indicates that in graphene

coated interconnect, owing to the lower resistance and current density, the same amount of current is transferred longer distance compared to uncoated one.
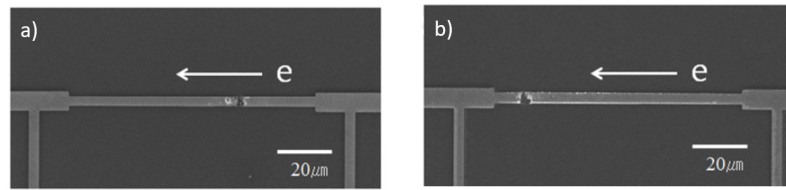
Figure 1.7. A comparison of the resistance of Cu and MLG/Cu interconnects.
(Source: Kang et al., 2013)

In our work, we studied the question of how we could improve the high heat removal performance on the computer processors. According to previous studies thermal performance graphene coated copper system gives high heat removal performance. Consequently, fabricated four different samples as a pure copper foil (Cu), annealed copper foil (An-Cu), single-layer graphene coated (SLG-Cu) and, multi-layer graphene coated copper foil (MLG-Cu) were investigated. Then, they were compared depending on the different flow rates $50\ ml/min$, $75\ ml/min$ and, $100\ ml/min$ based on temperatures $40°C$, $60°C$, and $80°C$ to see the effect on the thermal performances of them.

1.1.2. Molecular Dynamics Simulation of Graphene Coated Copper

There are number of studies about to investigate the thermal conductivity of the graphene and graphene-coated materials numerically and MD simulation program is one of them.

MD provides an atomistic level understanding of materials properties and it is widely used in chemical physics, materials science and molecular-scale modelling (Mortazavi et al., 2012). Basically, it is a simulation program, which computes the physical movements of atoms by using Newton's equation of motion and from these motions to obtain detailed information about atoms and molecules behavior with the calculating physical and chemical properties together (Frenkel and Smit, 2001).

In late of 1950's, Alder and Wainwright (1959) first presented the molecular dynamics method to study the interactions of atoms in the many-body systems. After that, In 1964, Rahman (1964) succeeds in a realistic potential for simulating the liquid argon. His system consists of 864 particles and these particles interact with each other with Lennard-Jones (LJ) potential by obeying the Newton's equations of motion. In 1974, Stillinger

and Rahman (1974) done the first molecular dynamics simulation of a realistic system of liquid water.

There are numerous potentials have been using in classical MD simulation to calculate thermal conductivity. When the previous studies have investigated to model graphene-coated copper system, it has seen that the commonly used potentials as shown in Figure 1.8.
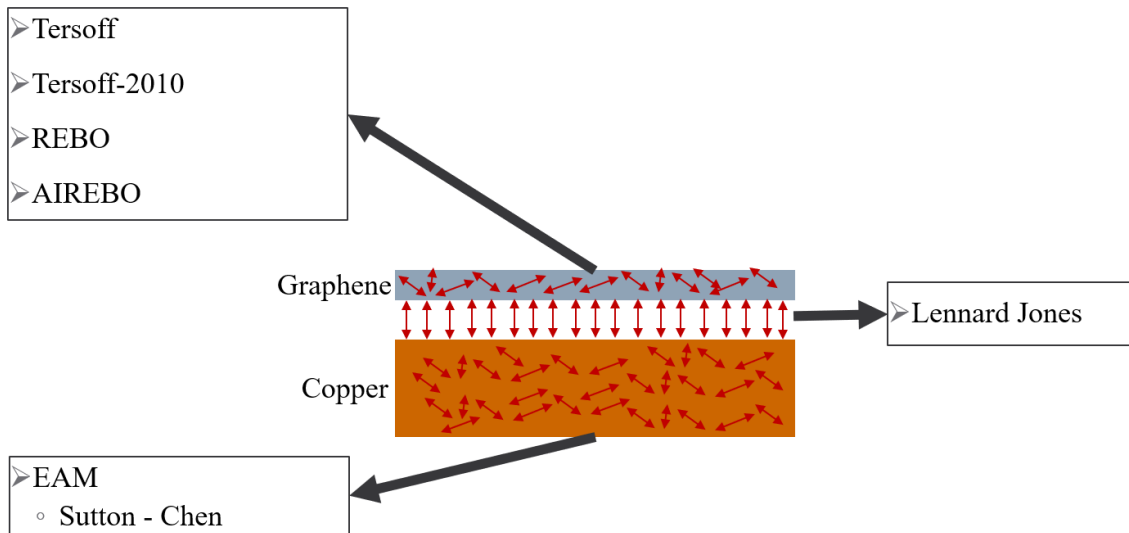
Figure 1.8. Potential Energy Functions for graphene coated copper.

As shown in above, LJ is used for non-bonded atoms like graphene and copper atoms interactions. The Sutton-Chen potential (Sutton and Chen, 1990), which is a version of Embedded Atom Modelling (EAM), is modeled for metal atoms like copper. In the literature, for graphene modeling, there are four commonly used potential energy functions which are called Tersoff (Tersoff, 1988), Tersoff-2010 (Optimized Tersoff) (Lindsay and Broido, 2010), Reactive Epirical Bond Order (REBO) ((Brenner et al., 2002)), and Adaptive Intermolecular Reactive Empirical Bond Order potential (AIREBO) (Stuart et al., 2000).

Investigating the impacts of these potentials on the thermal conductivity, Si et al. (2017) examined the interactions between the carbon atoms in graphene structure using MD. According to this research, three potentials, which are the Tersoff and the REBO, and the AIREBO significantly underestimate thermal conductivities of single-layer graphene. They reported that the opt-Tersoff (Tersoff-2010) is the most suitable potential for modeling both single and multi-layer graphene compare to others.

Researchers have found that the thermal conductivity of graphene increases with

the length using MD. This is called strong size dependence because of the long phonon mean free path (PMFP) of graphene, which is about 700-800 nm (Ghosh et al., 2008), and converge the thermal conductivity values near it (Mortazavi and Ahzi, 2012; Pop et al., 2012; Zhu et al., 2017; Guo et al., 2009; Wei et al., 2011; Si et al., 2017; Zhu et al., 2017; Guo et al., 2009; Cao et al., 2012; Yu and Zhang, 2013). Table 1.1 shows the length-dependent results of the thermal conductivity using commonly used potentials in MD.

Table 1.1. Thermal conductivity investigation of single-layer graphene and few-layer graphene respect to length changing with commonly used potential in MD.

Researchers	Model Type	Potential	Model Size (width x length)	Thermal Conductivity W/mK
Yu and Zhang, 2013	SLG	The TERSOFF	10 nm x 100 nm	~368
			10 nm x 600 nm	~564
Si et al, 2017	SLG	The TERSOFF	5 nm x 17 nm	~165
			5 nm x 50 nm	~309
		The TERSOFF-2010	5 nm x 17 nm	~238
			5 nm x 50 nm	~440
		The AIREBO	5 nm x 17 nm	~114
			5 nm x 50 nm	~216
		The REBO	5 nm x 17 nm	~79
			5 nm x 50 nm	~131
	2 layer Graphene	The TERSOFF	5 nm x 17 nm	~164
			5 nm x 50 nm	~308
		The TERSOFF-2010	5 nm x 17 nm	~194
			5 nm x 50 nm	~382
		The AIREBO	5 nm x 17 nm	~114
			5 nm x 50 nm	~225
		The REBO	5 nm x 17 nm	~75
			5 nm x 50 nm	~130
Mortazavi and Ahzi, 2012	SLG	The TERSOFF-2010	3.7 nm x 50 nm	~416
			3.7 nm x Infinite	~3000
Zhu et al, 2017	SLG	The REBO	3.9 nm x 12 nm	~228
			3.9 nm x 48 nm	~475
Guo et al, 2009	SLG	The TERSOFF	2 nm x 11 nm	~472
			2 nm x 60 nm	~864
Wei et al, 2011	SLG	The TERSOFF	2.84 nm x 7 nm	~128
			2.84 nm x 25 nm	~292
Cao et al, 2012	SLG	The TERSOFF	2 nm x 10 nm	~495
	2 layer Graphene			~396
	3 layer Graphene			~348
	4 layer Graphene			~309
	5 layer Graphene			~297

In addition, it is demonstrated that the thermal conductivity of graphene affected by the increment in the width direction (Zhu et al., 2017; Guo et al., 2009; Cao et al., 2012)

9

which is indicated in Table 1.2. This is because the reduction of edge localized phonon effect. In addition to that when the width increases then boundary scattering effect will decrease, and which leads to enhancement the thermal conductivity.

Table 1.2. Thermal conductivity investigation of single-layer graphene and few-layer graphene respect to width changing with commonly used potential in MD.

Researchers	Model Type	Potential	Model Size (width x length)	Thermal Conductivity W/mK
Zhu et al, 2017	SLG	The REBO	3.9 nm x 12 nm	~228
			6 nm x 12 nm	~235
			8 nm x 12 nm	~244
Guo et al, 2009	SLG	The TERSOFF	4.26 nm x 11 nm	~471
			8.52 nm x 11 nm	~503
			12.78 nm x 11 nm	~530
Cao et al, 2012	SLG	The TERSOFF	1 nm x 10 nm	~467
			2 nm x 10 nm	~490
			4 nm x 10 nm	~511
			8 nm x 10 nm	~513
	2 layer Graphene		1 nm x 10 nm	~324
			2 nm x 10 nm	~338
			4 nm x 10 nm	~363
			8 nm x 10 nm	~354

Furthermore, temperature dependence of thermal conductivity is investigated (Zhu et al., 2017; Momenzadeh et al., 2013). Increasing the temperature of the system cause a problem of the movement of atoms and leads to increase phonon scattering which resulted to reduce thermal conductivity.

The thermal conductivity of the graphene and carbon-based material on metal model is studied using MD are examined as follows. Wejrzanowski et al. (2015) investigated the heat transfer mechanism through from metal to graphene that is Cu and Ag composites with SLG and MLG graphene by using molecular dynamics simulation. They performed the simulation with LAMMPS sofware. EAM potential was used for modeling Cu-Cu and Ag-Ag interactions.AIREBO potential was used for C-C interactions in graphene. Non-bonding interactions between graphene and metals, were described with Lennard-Jones potential. The results show that interfacial thermal resistance (ITR) between metal and graphene significantly higher for SLG-Ag than for SLG-Cu. Moreover, they found that the ITR decreases with an increase in the number of graphene layers.

Next year, same researchers studied about SLG and MLG graphene for thermal conductivity enhancement (TCE) of copper numerically using ANSYS. The calculations

were carried out using the Finite Element Method (FEM). The results show that SLG to the copper didn't enhance the macroscopic thermal conductivity, it decreased the thermal expansion coefficient and friction coefficient. However, it increased the mechanical strength of copper. On the other hand, it suggested that thermal enhancement can be obtained by adding MLG to copper (Wejrzanowski et al., 2016).

All mentioned previous studies use to calculate thermal conductivity non equilibrium molecular dynamics simulation (NEMD). The simulation uses the heat source and the heat sink in the thermal conductivity calculations. As a different method Chen and Kumar (2012) investigate the thermal transport in single layer graphene and supported on copper using equilibrium molecular dynamics simulation. In the Green-Kubo method, periodic boundaries are effective. On the other hand, the size effect is crucial in NEMD. Also, the size effect impact in Green-Kubo method is much lower than NEMD.

Researchers used Tersoff-2010 and EAM potential to describe the C-C interactions and Cu-Cu interactions, respectively. The van der Waals interaction between non-bonded C-Cu atoms is modeled by Lennard-Jones potential. They found single layer graphene and graphene coated copper's thermal conductivity respectively 1779 W/mK and 1281.5 W/mK. Their results show that the thermal conductivity of graphene decreases by 44%. It can be said that thermal conductivity of graphene reduces when coated. However, it can be said that due to the high thermal conductivity of graphene, the thermal conductivity of copper was enhanced.

Sharma et al. (2017) examined the effect of nano-reinforced SLG and carbon nanotube in the copper on the thermal conductivity by using MD. They performed MD simulation using condensed phase optimized molecular potential for atomistic simulation studies (COMPASS) software. The results demonstrated that under uniaxial tensile loadings, SLG-Cu performed better than CNT-Cu in terms of enhancing the mechanical properties. Moreover, when carbon (C) concentration is enhanced in both SLG and CNT, the thermal conductivity of SLG-Cu increased by 39% compared to the CNT-Cu that is only 27%.

As a different study, Mortazavi and Ahzi (2012) investigated the effects of boron atoms addition on the thermal conductivity of single-layer graphene using the NEMD simulations. They used LAMMPS and modeled the interaction between carbon atoms using the Optimized Tersoff Potential and for boron atoms were modeled using Tersoff Potential. The results suggest that the thermal conductivity of graphene along the zigzag direction takes a higher value than along the armchair direction. This can be explained by along the zigzag direction there are more phonons conduct heat than along the armchair direction. It was also observed that the thermal conductivity of graphene reduces with

only 0.75% concentration of boron atoms. This shows that when graphene interacts with another material, it causes a reduction in its thermal properties.

In this study, our motivation is to calculate the thermal conductivity numerically at different temperatures, lengths, width, and height of the graphene and the graphene-coated copper systems as writing a NEMD simulation code. The previous studies show that, in nanoscale level, the thermal conductivity is affected by some conditions like edge type, length, width, height, heat flux direction, boundary scattering effect, materials structure, boundary conditions, and etc. directly. For this reason, our aim to investigate these conditions using MD.

CHAPTER 2

MOLECULAR DYNAMICS SIMULATIONS OF
GRAPHENE-COATED COPPER

In this chapter, a C++ code is initially generated to create the lattice models of pure graphene, pure copper, and graphene-coated copper. After obtaining these models, the NEMD simulation code is generated to investigate the thermal conductivity of these materials. The effect of temperatures, lengths (x direction), width (y direction), and height (z direction) on the graphene, the copper, and the graphene-coated copper materials analyzed.

2.1. Molecular Dynamics

Molecular dynamics (MD) simulation is one of the numerical calculation methods. It provides an atomistic level understanding of materials properties and it is widely used in chemical physics, materials science and molecular-scale modelling. Basically, it is a simulation program, which computes the physical movements of atoms by using given as below Newton's equation of motion to obtain detailed information of behaviour of atoms and molecules with the calculating physical and chemical properties together .

$$F_i = m_i \frac{d^2 r_i}{dt^2}, \quad (i = 1, 2, 3, \dots, N) \tag{2.1}$$

In the equation, F_i is the force between atoms, m_i is mass of an atom, and $\frac{d^2 r_i}{dt^2}$ is time-dependent derivative of the position of $i.$ atom which is acceleration of an $i.$ atom. The aim of the MD is to solve this equation numerical method and obtain useful information from the atomic trajectories. Commonly used softwares for MD are LAMMPS, GROMACS NAMD, AMBER, etc.

In molecular dynamics, atom speeds and positions can be read any desired time. However, a typical experimental study cannot have a detail information like MD. It gives an average value about studied properties. Thus, MD simulation is one of the fast and useful computational method for studying behavior of atoms and molecules.

MD simulations are very similar to real experiments' preparations stage. The following figure displays the MD simulation basically.
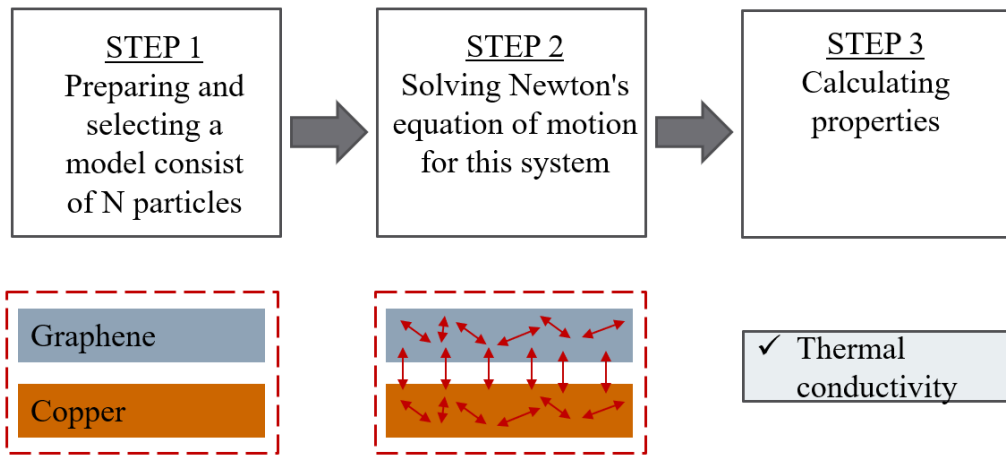
Figure 2.1. Simple MD Diagram for graphene-coated copper model.

First of all, the model is selected and prepared. Then to calculate forces between particles, Newton's equations of motion are solved. And finally, some properties such as temperature distribution are calculated.

Before running MD simulations, it is essential to choose one or more appropriate force fields that could well describe the interactions between atoms in the system.

2.1.1. Force Fields in Molecular Dynamics

In MD, molecules consist of atoms and bonds between them. Force fields are used to describe this relation between them. These force potentials in the literature are obtained from the numerical differentiation of the potential energy function respect to the distance between atoms.
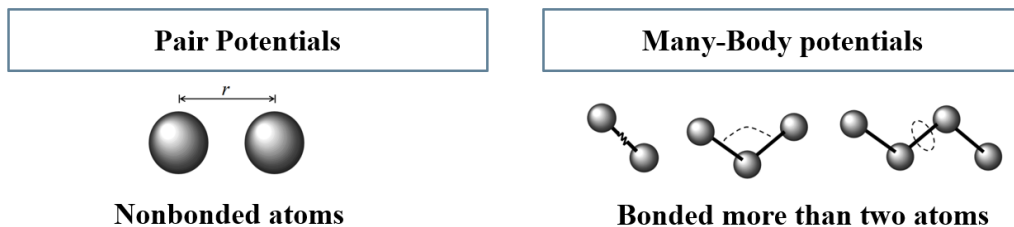
Figure 2.2. Potential energy functions.

The potential energy function can be separated as shown in Figure 2.2 into two main part. These are called "Pair Potential" and "Many-body Potential". Pair potentials

calculates the interaction between non-bonded atoms like metals or C-Cu interactions in graphene coated copper model. Many-body potential calculates the interaction between bonded two or more than two atoms like graphene. They determine the change in bond lengths, bond angle, torsion and non-bonding interactions between atoms. Then, sum up these calculated potential to obtain the total energy of the atoms from equation 2.2.

$$U\left(r_1, r_2, r_N\right) = \sum_i U_1\left(r_i\right) + \sum_{j>i}\sum_i U_2\left(r_i, r_j\right) + \sum_i\sum_{j>i}\sum_{k>j} U_3\left(r_i, r_j, r_k\right) + \dots \quad (2.2)$$

U_1 =Energy of 1 atom system, U_2 =Energy of 2 atom system, U_3 =Energy of 3 atom system, U_N =Energy of N atom system

As mentioned in previous chapter, to describe C-C interaction for graphene modeling there are four potential energy function in the literature. In this study Tersoff Potential is used due to better describe various chemical reactions and calculation speed in large systems. Also, this potential gives better description of bond energies, lengths, angle and force between atoms.

Tersoff Potential is one of the most commonly used potential, especially for carbon-based systems (Tersoff, 1988). It calculated the atomic interaction between three atoms based on their bond angle and distance which is indicated in Figure 2.3. Then the total energy of atoms in the system defines as U_{ij}.

$$E = \sum_i E_i = \frac{1}{2}\sum_{i\neq j} U_{ij} \quad (2.3)$$
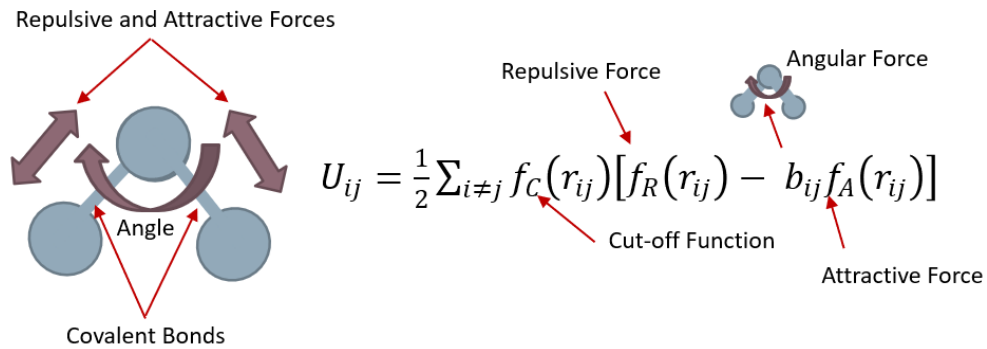
Figure 2.3. Representative showing of Tersoff Potential and energy equation.

Here E is the total energy of the system. Then i, and j are label of the atoms in the system, r_{ij} is the distance of the bonded atoms. f_C represents the cut off function. f_R and f_A is called attractive and repulsive terms respectively. The term, b_{ij} term describes the angular forces between atoms. Angular force keeps atom equilibrium angle.

15

The force on each atom must be calculated in order to examine the interactions between the carbon atoms in graphene. The energy (U_{ij}) must be derived from respect to the position for the calculation of the force on each atom. The calculations are made to obtain derivation of the Tersoff Potential are given below and used variables given in Table 2.1.

$$E_i = \frac{1}{2} \sum_{i \neq j} U_{ij} = \frac{1}{2} \sum_{i \neq j} f_c(r_{ij}) \left[f_R(r_{ij}) - b_{ij} f_A(r_{ij}) \right] \tag{2.4}$$

$$
\begin{aligned}
f_i = -\frac{dU_{ij}}{dr_{ij}} = &-\frac{1}{2} \sum_{i \neq j} f_C'(r_{ij}) \left[f_R(r_{ij}) - b_{ij} f_A(r_{ij}) \right] \\
&+ f_C(r_{ij}) \left[f_R'(r_{ij}) - b_{ij}' f_A(r_{ij}) - b_{ij} f_{A(r_{ij})}' \right]
\end{aligned} \tag{2.5}
$$

$$f_R = A \exp(-\lambda_{ij} r_{ij}) \qquad f_R' = -A \lambda_{ij} \exp(-\lambda_{ij} r_{ij}) \tag{2.6}$$

$$f_A = B \exp(-\mu_{ij} r_{ij}) \qquad f_A' = -B \mu_{ij} \exp(-\mu_{ij} r_{ij}) \tag{2.7}$$

$$f_C = \begin{cases} 1 & r_{ij} < R \\ \frac{1}{2}(1 + cos(\pi(r_{ij} - R)/(S - R))) & R < r_{ij} < S \\ 0 & r_{ij} > S \end{cases} \tag{2.8}$$

$$f_C' = \begin{cases} 0 & r_{ij} < R \\ -\frac{\pi}{2(S-R)}(sin(\pi(r_{ij} - R)/(S - R))) & R < r_{ij} < S \\ 0 & r_{ij} > S \end{cases} \tag{2.9}$$

$$b_{ij} = \left(1 + \beta^n \xi_{ij}^n\right)^{-1/2n} \qquad and \qquad \xi_{ij} = \sum_k f_C(r_{ij}) g(\theta_{ijk}) \tag{2.10}$$

$$\frac{db_{ij}}{dr_{ij}} = \frac{db_{ij}}{d\xi_{ij}} \cdot \frac{d\xi_{ij}}{dr_{ij}} \tag{2.11}$$

$$\frac{db_{ij}}{d\xi_{ij}} = -\frac{1}{2n}(1 + \beta^n \xi_{ij}^n)^{\frac{-1}{2n} - 1}(n\beta^n \xi_{ij}^{n-1}) \tag{2.12}$$

$$\frac{d\xi_{ij}}{dr_{ij}} = f_C'(r_{ij}) g(\theta_{ijk}) + f_C(r_{ij}) g'(\theta_{ijk}) \tag{2.13}$$

$$g(\theta_{ijk}) = 1 + \frac{c^2}{d^2} - \frac{c^2}{d^2 + (h - cos(\theta_{ijk}))^2} \tag{2.14}$$

$$g'(\theta_{ijk}) = \frac{dg}{d\theta_{ijk}} = 2c^2 \left[d^2 + (h - cos(\theta_{ijk}))^2 \right]^{-2} (h - cos(\theta_{ijk})) sin(\theta_{ijk}) \tag{2.15}$$

16

$$\frac{dg}{dcos(\theta_{ijk})} = -2c^2 \left[d^2 + (h - cos(\theta_{ijk}))^2 \right]^{-2} \tag{2.16}$$

Since the Tersoff Potential calculate length between the two atoms and the angular balance between the three atoms, three different forces (F_i, F_j and F_k) applied to the i, j and k atoms are calculated as follows.

$$F_i = -\frac{1}{2} \sum_j \{ f'_C(r_{ij}) [f_R(r_{ij}) - b_{ij} f_A(r_{ij})]$$
$$+ f_C(r_{ij}) [-\lambda_{ij} f_R(r_{ij}) + \mu_{ij} b_{ij} f_A(r_{ij})] \} \frac{\mathbf{r}_{ij}}{r_{ij}} \tag{2.17}$$
$$+ \frac{1}{2} \sum_j c^1_{ij} f_C(r_{ij}) f_A(r_{ij}) \frac{\partial \xi_{ij}}{\partial \mathbf{r}_i}$$

$$F_j = -\frac{1}{2} \sum_j \{ f'_C(r_{ij}) [f_R(r_{ij}) - b_{ij} f_A(r_{ij})]$$
$$+ f_C(r_{ij}) [-\lambda_{ij} f_R(r_{ij}) + \mu_{ij} b_{ij} f_A(r_{ij})] \} \frac{\mathbf{r}_{ij}}{r_{ij}} \tag{2.18}$$
$$+ \frac{1}{2} \sum_j c^1_{ij} f_C(r_{ij}) f_A(r_{ij}) \frac{\partial \xi_{ij}}{\partial \mathbf{r}_j}$$

$$F_k = \frac{1}{2} c^1_{ij} f_{C_{ij}} f_{A_{ij}} \frac{\partial \xi_{ij}}{\partial \mathbf{r}_k} \tag{2.19}$$

$$c^1_{ij} = -\frac{1}{2} \beta_i (\beta_i \xi_{ij})^{n-1} \left(1 + \beta_i^n \xi_{ij}^n \right)^{\frac{-1}{2n} - 1} \tag{2.20}$$

$$\frac{\partial \xi_{ij}}{\partial \mathbf{r}_i} = \sum_k \left\{ g f'_C(r_{ik}) \frac{\mathbf{r}_{ik}}{r_{ik}} + c^2_{ij} (\cos \theta_i) \right\} \tag{2.21}$$

$$\frac{\partial \xi_{ij}}{\partial \mathbf{r}_j} = \sum_k c^2_{ij} (\cos \theta_j) \tag{2.22}$$

$$\frac{\partial \xi_{ij}}{\partial \mathbf{r}_k} = \left\{ -g f'_C(r_{ik}) \frac{\mathbf{r}_{ik}}{r_{ik}} \right\} + c^2_{ij} (\cos \theta_k) \tag{2.23}$$

$$c^2_{ij} = f_C(r_{ik}) \frac{-2c^2 (h - \cos(\theta_{ijk}))}{\left[d^2 + (h - \cos(\theta_{ijk}))^2 \right]^2} \tag{2.24}$$

$$\cos(\theta_{ijk})_i = \left\{ \frac{1}{r_{ik}} - \frac{\cos(\theta_{ijk})}{r_{ij}} \right\} \frac{\mathbf{r}_{ij}}{r_{ij}} + \left\{ \frac{1}{r_{ij}} - \frac{\cos(\theta_{ijk})}{r_{ik}} \right\} \frac{\mathbf{r}_{ik}}{r_{ik}} \tag{2.25}$$

$$\cos(\theta_{ijk})_j = \left(\frac{\cos(\theta_{ijk})}{r_{ij}} \frac{\mathbf{r}_{ij}}{r_{ij}} \right) + \left(-\frac{1}{r_{ij}} \frac{\mathbf{r}_{ik}}{r_{ik}} \right) \tag{2.26}$$

17

$$\cos\left(\theta_{ijk}\right)_k = \left(-\frac{1}{r_{ik}}\frac{\mathbf{r}_{ij}}{r_{ij}}\right) + \left(\frac{\cos\left(\theta_{ijk}\right)}{r_{ik}}\frac{\mathbf{r}_{ik}}{r_{ik}}\right) \tag{2.27}$$

Table 2.1. Tersoff Potential variables for graphene (Tersoff, 1988)

Parameters	Values
A [kcal/mol]	32137,17
B [kcal/mol]	7996,012
λ [Å^{-1}]	3,4879
μ [Å^{-1}]	2,2119
R [Å]	1,8
S [Å]	2,1
n [-]	0,72751
c [-]	38049,0
β [-]	1,5724x10^{-7}
d [-]	4,3484
h [-]	-0,57058

In the literature, EAM is widely used for the modeling of the metals, and Sutton-Chen potential is one of the version of EAM (other versions are Finnis –Sinclair, Voter-Chen etc..). Also, researchers used Lennard-Jones (LJ) potential for the modeling of metals. However, LJ doesn't well define the relationship between metal atoms as much as Sutton-Chen. Further, its error margin was more than Sutton-Chen.

Kang et al. (2011) modeled copper with the potential of Lennard Jones and Sutton-Chen. Then, they calculated the thermal conductivity of copper. In their results, the thermal conductivity of copper was found to show less oscillation in Sutton-Chen potential compared to the LJ.

Sutton-Chen is based on a density functional theory. The energy of the metal atoms shown in the Figure 2.4 is defined by the local electron density which creates an the embedding energy. This energy describes the metal atoms behavior well because it calculate each atom density in the system. The following energy equation of Sutton-Chen describes the interaction between atoms based on their distance (r_{ij}) and the total electron density (ρ_i) .

$$E_i = U_{ij} = \varepsilon \left[\frac{1}{2}\sum_{j\neq i}\left(\frac{a}{r_{ij}}\right)^n - c\sqrt{\rho_i}\right], \quad \rho_i = \sum_{j\neq i}\left(\frac{a}{r_{ij}}\right)^m \tag{2.28}$$

In the equation, ε is a parameter of energy, a is the lattice constant, c is a dimensionless parameter, m and n are positive integers with n > m.
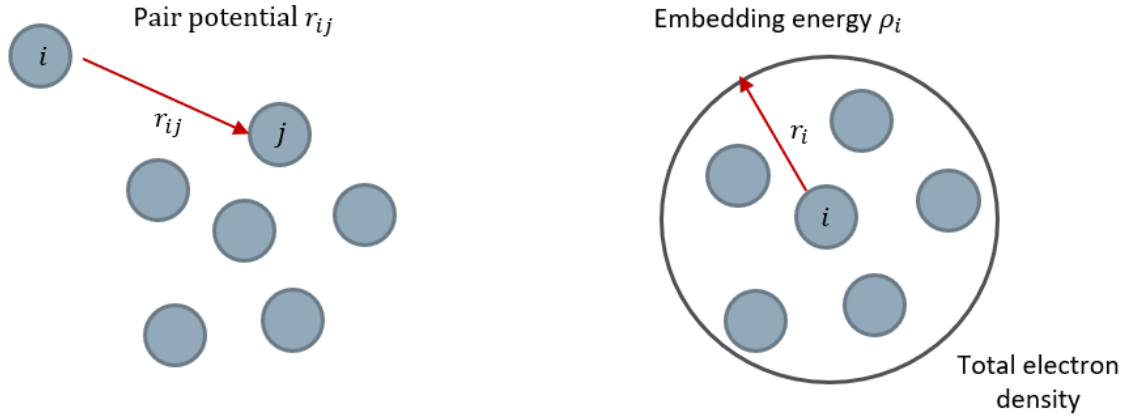
Figure 2.4. Embedded energy and total electron density in Sutton-Chen potential.

The force on each atom in copper is calculated using the following formulas which are the derivation of Sutton-Chen Potential respect to the position. The used variables are given in Table 2.2.

$$f_k = -\frac{dU_{ij}}{dr_{ik}} = -\varepsilon \left[n \left(\frac{a}{r_k} \right)^n - \frac{c \cdot m}{2} \left(\frac{1}{\sqrt{\rho_k}} + \frac{1}{\sqrt{\rho_i}} \right) \left(\frac{a}{r_k} \right)^m \right] \left(\frac{1}{r_k} \right) \tag{2.29}$$

Table 2.2. Sutton-Chen potential variables for copper (Sutton and Chen, 1990).

Parameters	Values
ε [kcal/mol]	0,28553563
a [Å]	3,61
c [-]	39,432
m [-]	6
n [-]	9

Among all pair potentials, one of the most famous one in the literature is LJ potential for non-bonding atoms due to its computational simplicity and accuracy in computer simulations. The interactions between graphene-copper (C-Cu) and graphene layers (C-C) are calculated by LJ with the parameters in Table 2.3. The following energy equation of LJ describes the interaction between atoms based on their distance.

$$U_{ij} = 4\varepsilon \left[\left(\frac{\sigma}{r_{ij}} \right)^{12} - \left(\frac{\sigma}{r_{ij}} \right)^6 \right] \tag{2.30}$$

where ε is the bonding energy indicates to the inter-atomic energy between two atoms at the equilibrium distance, σ is the distance between two atom where potential

Table 2.3. Lennard-Jones potential variables for C-Cu and C-C (Sidorenkov et al., 2016; Lebedeva et al., 2011).

Parameters for C-Cu	Values
σ [Å]	2.2
ε [kcal/mol]	0,3874171
r_{cutoff} [Å]	2,5σ
Parameters for C-C	**Values**
σ [Å]	3,93
ε [kcal/mol]	0,0635779141
r_{cutoff} [Å]	3,0σ

is equal to zero, and r_ij is the distance between atoms. If the distance between the two atoms is more than equilibrium distance, atoms are pulling each other by attractive forces otherwise if the atoms are very close to each other, repulsive forces push the atoms from each other trying to move to the atoms equilibrium position as shown in Figure 2.5.
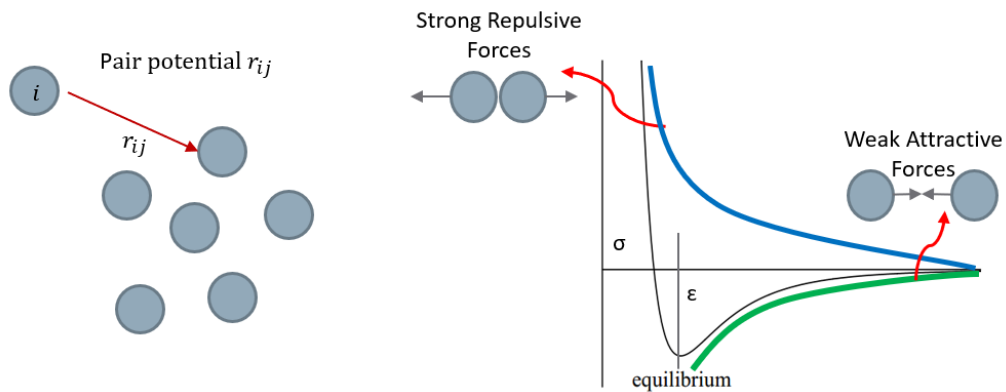
Figure 2.5. Representation of the Lennard-Jones potential energy curve.

The forces were obtained derivation of the equation 2.30 with respect to the distance of between the graphene-copper atoms.

$$f_i = -\frac{dU_{ij}}{dr_{ij}} = \frac{48}{r_{ij}}\varepsilon \left(\frac{\sigma}{r_{ij}}\right)^6 \left[\left(\frac{\sigma}{r_{ij}}\right)^6 - \frac{1}{2}\right] \qquad (2.31)$$

As showing in the following equation, It is important to calculate the interaction of the atoms remaining within the cut-off distance and ignore the others because of the importance of calculation time.

$$f_i = \left\{ \frac{48}{r_{ij}} \varepsilon \left(\frac{\sigma}{r_{ij}} \right)^6 \left[\left(\frac{\sigma}{r_{ij}} \right)^6 - \frac{1}{2} \right] \right\}$$
$$- \left\{ \frac{48}{r_{\text{cutoff}}} \varepsilon \left(\frac{\sigma}{r_{\text{cutoff}}} \right)^6 \left[\left(\frac{\sigma}{r_{\text{cutoff}}} \right)^6 - \frac{1}{2} \right] \right\} \qquad if \quad r_{ij} > r_{cutoff} \qquad (2.32)$$

The potential energy of LJ calculated according to the equation 2.30 can be seen in Figure 2.6. When σ is equal to 2.2, potential energy is equal to zero which means that the interaction between atoms switches from being attractive ($r_ij > \sigma$) to repulsive ($r_ij < \sigma$).
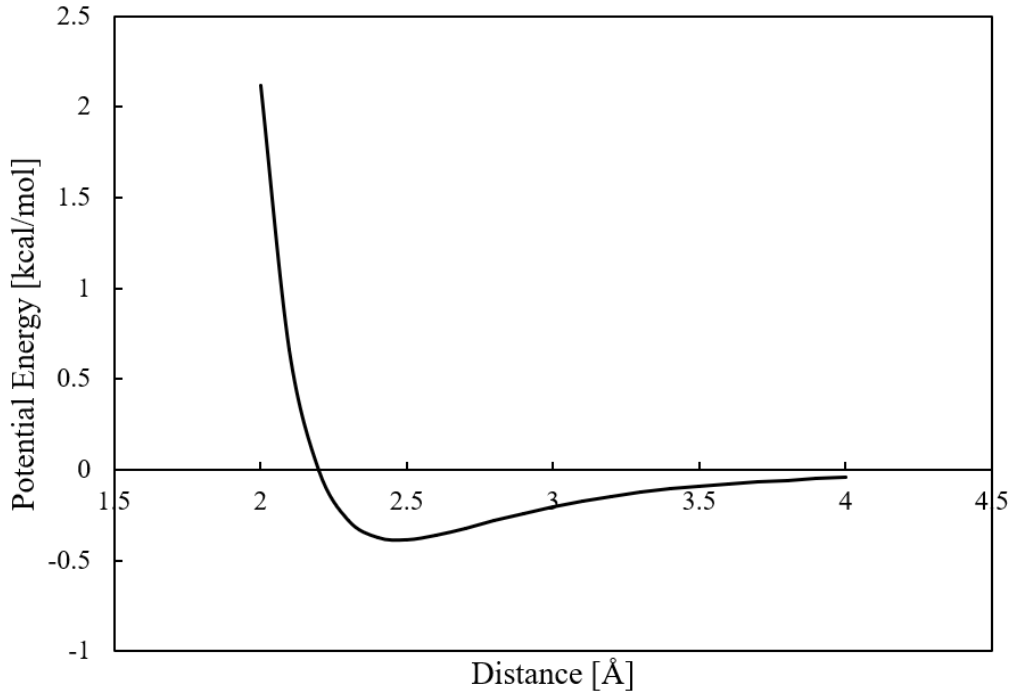
Figure 2.6. Copper-Graphene surface Lennard-Jones potential energy function.

2.1.2. Integration Algorithms

After calculating the inter-atomic forces within the model, the acceleration of the atoms using the $F = ma$ equation, which is the second law of Newton, were calculated. In this equation, m is the mass of the atoms and a is the acceleration of the atoms. After calculating the acceleration of atoms, the velocities and positions of atoms in three dimensional systems are updated by calculating the time integration of the acceleration by a numerical method. In this study, Velocity Verlet algorithm which is one of the numerical

integral calculation methods was used. The purpose of this algorithm is to obtain system conditions at time t + dt from the system conditions at time t in two time periods (t+ dt/2) for velocities which is called leap frog method. The logic of the algorithm is shown in Figure 2.7.
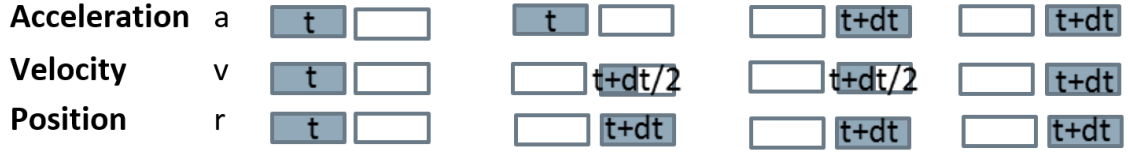
Figure 2.7. Schematic diagram of velocity verlet algorithm.

Velocity Verlet algorithm was used because its algorithm has a simple writing, high accuracy (second order), and high computational speed that required in MD. The integration algorithm (positions, velocities and accelerations)comes from the Taylor series expansion:

$$r(t + dt) = r(t) + v(t)dt + \frac{1}{2}a(t)dt^2 + \dots \tag{2.33}$$

$$v(t + dt) = v(t) + a(t)dt + \frac{1}{2}h(t)dt^2 + \dots \tag{2.34}$$

$$a(t + dt) = a(t) + h(t)dt + \dots \tag{2.35}$$

To derive the Velocity Verlet algorithm that can be written using the central difference method with Taylor expansion as follow:

Firstly, position is written using forward difference method.

$$r(t + dt) = r(t) + v(t)dt + \frac{1}{2}a(t)dt^2 \tag{2.36}$$

Then, it is written using backward difference method.

$$r(t - dt) = r(t) - v(t)dt + \frac{1}{2}a(t)dt^2 \tag{2.37}$$

To sum up these two equations,

$$r(t + dt) = 2r(t) - r(t - dt) + a(t)dt^2 \tag{2.38}$$

From the central difference method, equation of velocity is obtained.

$$v(t) = \frac{r(t + dt) - r(t - dt)}{2dt} \tag{2.39}$$

22

The velocity equation is substituted by the backward part of the position in equation 2.38.

$$r(t + dt) = 2r(t) + 2v(t)dt - r(t + dt) + a(t)dt^2 \tag{2.40}$$

As a result of the simplification, the position equation of the Velocity Verlet algorithm is obtained.

$$r(t + dt) = r(t) + v(t)dt + \frac{1}{2}a(t)dt^2 \tag{2.41}$$

After the obtained position equation, other steps of the Velocity Verlet algorithm is demonstrated as follows:

- Calculation of atoms' velocities v at half of the next iteration time $t + dt/2$,
  $v(t + dt/2) = v(t) + a(t)dt/2$
- Calculation of atoms' positions x at the next iteration time $t + dt$,
  $r(t + dt) = r(t) + v(t + dt/2)dt$
- Update of atoms' acceleration a by Force F based on Newton equation which is $F = ma$ at the next iteration time $t + dt$,
  $a(t + dt) = F(t + dt)/m$
- Finally, update of atoms' velocities v at next iteration time $t + dt$,
  $v(t + dt) = v(t + dt/2) + a(t + dt)dt/2$

2.1.3. Temperature Controls

After the modeling of graphene and copper, the calculation of the desired properties (in our case this is thermal conductivity), the temperature of the system must be calculated. In MD simulations, the temperature of the system calculated according to the following equipartition theorem.

The kinetic energy of the atoms in the system, due to the kinetic theory of gases is equal at thermal equilibrium. (eq. 2.42, 2.43)

$$E_{\text{kinetic}} = \sum_{i=1}^{N} \frac{1}{2}mV^2 \tag{2.42}$$

$$\sum_{i=1}^{N} \frac{1}{2}mV^2 = \frac{3}{2}k_B T \tag{2.43}$$

Then, temperature of the system is calculated as follow;

$$T = \frac{2E_{\text{kinetic}}}{3k_B} = m \sum_{i=1}^{N} \frac{V_i^2}{3k_B} \tag{2.44}$$

23

The Boltzmann constant (k_B) provides a connection between the microscopic and macroscopic system, by calculating the typical average kinetic energies of the microscopic system to change the temperature of a macroscopic system.

In MD situations, it is required to run simulations in the standard (NVT) ensemble involving temperature control. Expansion of NVT is a constant number (N), volume (V), and temperature (T). In order to keep the desired temperature, a thermostat must be applied to the system. Different thermostat algorithms are included in the literature, but thermostat selection is important in order to obtain accurate results in nano dimensions. For this reason, Nosé-Hoover Thermostat (Hoover, 1985). has been selected because easy to write its algorithm, have high sensitivity to control the system temperature and most used one among to others. This thermostat basically scales the kinetic energy of the system according to the desired temperature. Nosé-Hoover Thermostat (NH) algorithm calculated according to the combination of the NH and the reversible velocity Verlet integrator. According to the set temperature of the system new velocities and positions of the atoms are calculated at the next time step with following steps;

- Thermostat acceleration $\ddot{\xi}$ is calculated at t,
  $$\ddot{\xi}(t) = \frac{1}{\tau^2}\left[\frac{T(t)}{T_{set}} - 1\right]$$
- Thermostat velocity $\dot{\xi}$ is computed at $t + dt/2$,
  $$\dot{\xi}(t + dt/2) = \dot{\xi}(t) + \ddot{\xi}(t)dt/2$$
- Thermostat position ξ is calculated at $t + dt$,
  $$\xi(t + dt) = \xi(t) + \dot{\xi}(t + dt/2)dt$$
- Evolve particle velocities v at $t + dt/2$,
  $$v(t + dt/2) = v(t)e^{[-\dot{\xi}(t+dt/2)dt/2] + a(t)dt/2}$$
- Evolve particle positions x at $t + dt$,
  $$x(t + dt) = x(t) + v(t + dt/2)dt$$
- Compute acceleration of atoms a, according to Force F at $t + dt$,
  $$a(t + dt) = F(t + dt)/m$$
- Update the thermostat acceleration $\ddot{\xi}$ at $t + dt$,
  $$\ddot{\xi}(t + dt) = \frac{1}{\tau^2}\left[\frac{T(t+dt)}{T_{set}} - 1\right]$$
- Lastly, update the thermostat velocity $\dot{\xi}$ at $t + dt$,
  $$\dot{\xi}(t + dt) = \dot{\xi}(t + dt/2) + \ddot{\xi}(t + dt)dt/2$$

2.1.4. Parallel Computing - Message Passing Interface (MPI)

Parallel computing with disturbed memory is a method of solving complex calculations. MPI was designed for distributed or shared memory. In other words, it is used for programming systems where each process has a different address or when processors need to communicate each other. General structure of MPI program is shown Figure 2.8.
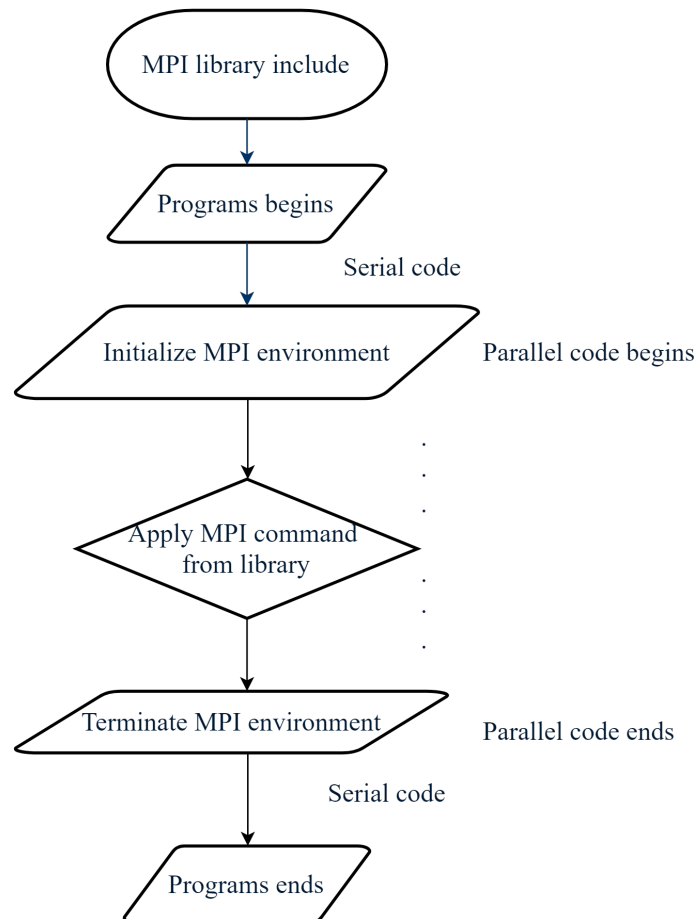
Figure 2.8. General MPI program structure.

In the MD code, firstly, an algorithm was written which atoms would be distributed to processors according to the number of processors to be used. This algorithm is used to determine which processor will calculate which atoms. Figure 2.9 schematically shows MPI logic.

This algorithm provides task allocation to the processors. Therefore, the calculations will be faster as the number of atoms assigned to each processor will be approximately equal. Also MPI provides a communication among the processors. For example, the calculated results are send or receive between the processors.
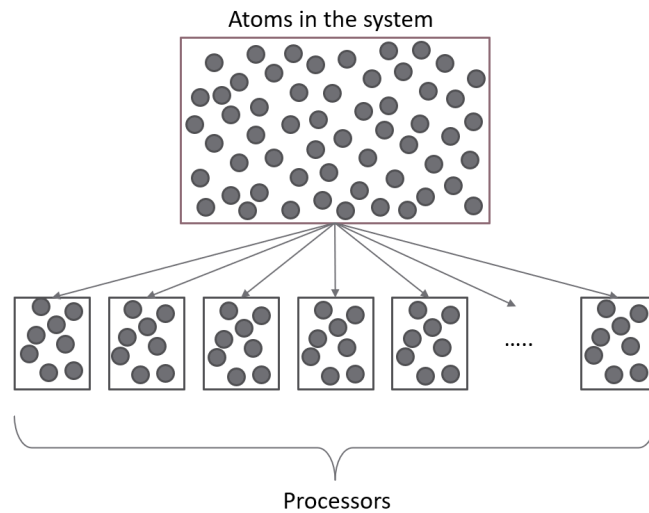
Figure 2.9. Representation of MPI logic.

2.2. Simulation Details

In this study all the simulations were performed writing an MD simulation code in C++ language. In MD, molecules consist of atoms and bonds between them. In Figure 2.10, the graphene-coated copper simulation model can be seen as an example.
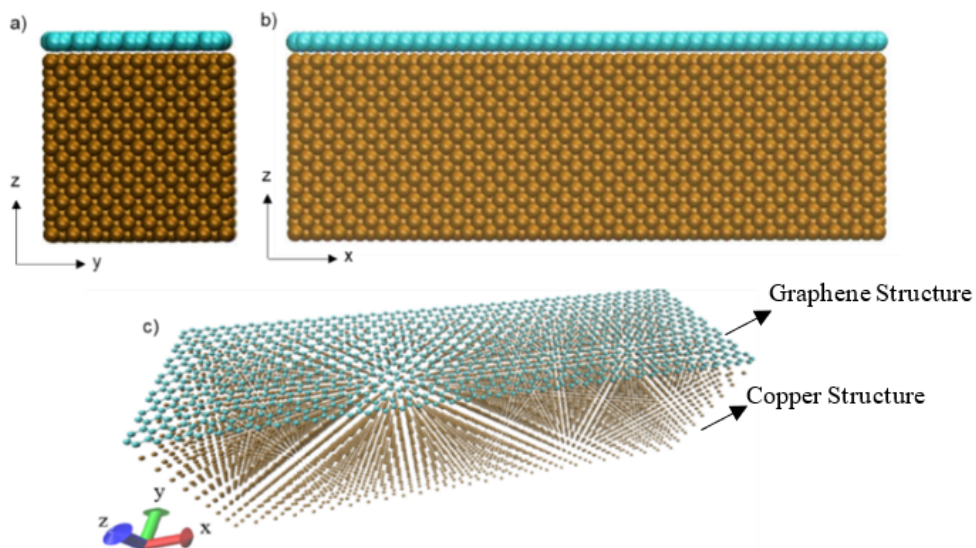
Figure 2.10. Representation of graphene-coated copper model. a) Side view, b) Front view, c) Showing bonding and non-bonding atoms in the simulation model.

Figure 2.11, presents the distance of the simulation models as x- (length), y- (width) and, z- (height) direction with various size. For investigating the length effect

on the thermal conductivity, length is increased in the x-direction from $3\,nm$ to $24\,nm$ with constant size in y- and z-direction which is 3 nm and 2 nm respectively. In the same way, to study the increment the width in the y-direction, width is changed from 1.5 nm to 12 nm with constant size in x- and z-direction which is 6 nm and 2 nm respectively. After that, height is extended in the z-direction from 2 nm to 8 nm to search the effect on the thermal conductivity with constant size in x- and y-direction which is 6 nm and 3 nm respectively.
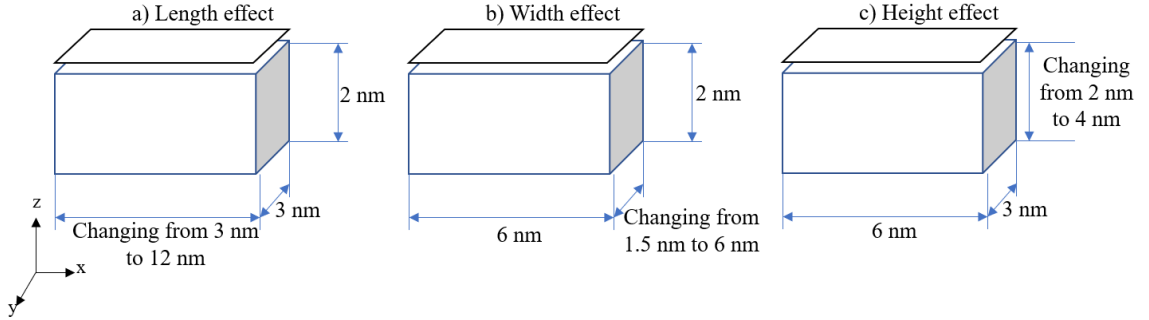
Figure 2.11. A schematic presentation of the simulation model with different size on the effect of the thermal conductivity a) Length effect, b) Width effect, c) Height effect.

In graphene, to create a lattice structure, between carbon atom distance take as $0.142\,nm$ and to describe the covalent bonding interactions between carbon atoms (C-C), Tersoff Potential is chosen (Tersoff, 1988). For multilayer graphene model, the distance between the graphene layers takes $0.335\,nm$. (Wei et al., 2011). The face-centered cubic structure is chosen for copper modeling (Cu100) and, the distance between copper atoms take $0.365\,nm$. In addition to that, for the metallic interactions between copper atoms, EAM Potential (Sutton-Chen) is selected (Hoover, 1985). For the weak Van der Waals interactions, Lennard-Jones (LJ) potential is applied to the non-bonding interactions among the graphene layers, and between the graphene layers and copper (Vera, 2014). Furthermore, the distance between graphene layer and the copper model set as $0.34\,nm$. Between the copper and the graphene layer interactions, Lennard-Jones parameters define as, $\sigma = 0.30825\,nm$, and $\epsilon = 0.2578\,eV$ and cutoff distance of r_c take as 2.5σ at truncated (Hong et al., 2015).

In this study zigzag graphene structure (ZGNR) is studied because, the thermal conductivity of graphene along the zigzag direction takes a higher value than along the armchair direction in the literature (Mortazavi and Ahzi, 2012; Guo et al., 2009). Time step of the simulation set as $0.05\,fs$ (femtosecond) and all simulations run to $1.5\,ns$

(nanosecond). During the iteration time, to obtain particle new positions, the velocity Verlet algorithm is used. This algorithm calculates new positions and velocities of the atoms at the next iteration time step from t to $t + dt$.

Fixed boundary conditions apply to both ends of the simulation model at $x - min$ and $x - max$ position, and free boundary conditions apply in $y-$ and $z-$ direction. Next to the fixed atoms, error slabs are located to prevent atoms mismatch, and to obtain temperature profile, the thermostat applies to the following two slabs as a heat source 320 K and heat sink 280 K. System temperature is controlled by the Nosé-Hoover Thermostat (Hoover, 1985). Figure 2.12 shows the schematic diagram of the simulation model.
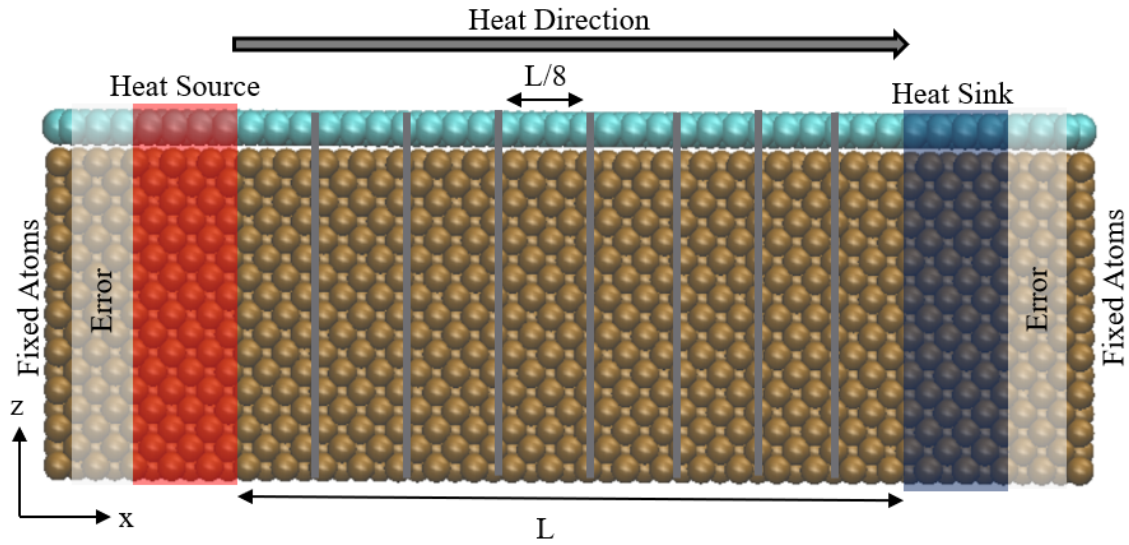
Figure 2.12. Schematic diagram of NEMD simulation of graphene-coated copper model.

The thermal conductivity calculation is performed using NEMD based on Fourier Law.

$$k = -\frac{J}{A(dT/dx)} \tag{2.45}$$

In the above formula, k is the thermal conductivity of the system, J is the heat flux, dT/dx is the temperature gradient, and A is the cross-section area in the direction of heat flux. Before the thermal conductivity calculation, the system temperature fixes at 300 K and relaxes with NVT (Canonical) ensemble which takes about $0.05\ ns$. After the system relaxed to the steady state NEMD simulation performed in NVE (micro-canonical) ensemble that runs up to final time step which is $1.5\ ns$. The simulation model divided into eight slabs to obtain a temperature profile excluding the error slabs and the thermostat slabs which is shown in Figure 2.13 as en example of a studied model. The temperature

of each slab is calculated using following equipartition theorem:

$$T_i = m \sum_{i=1}^{N} \frac{v_i^2}{3Nk_b} \quad (i = slab\ number) \tag{2.46}$$

In the above equation, T_i is the temperature of the ith slab, N is the total number of atoms in the ith slab, m is the mass of each atom and k_b is the Boltzmann constant.
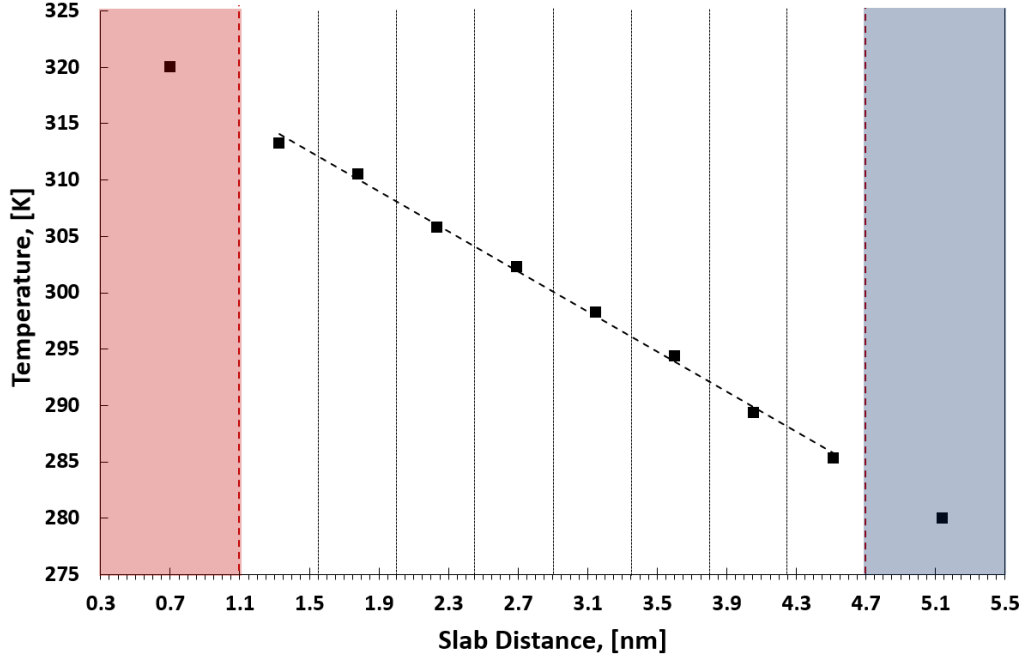
Figure 2.13. Temperature profile of a simulation model.

After the system relaxed to the steady state, the imposed thermostat heat flux method applied along the in-plane direction (x- direction) of the simulation model (Vera, 2014). In this method, kinetic energies of all atoms in the thermostat part are calculated before (old) and after (new) applying the thermostat with following the equations;

$$\Delta\varepsilon_{source} = \sum \frac{m}{2} \left(\sum_{Heat\ source} v_{new}^2 - \sum_{Heat\ source} v_{old}^2 \right) \tag{2.47}$$

$$\Delta\varepsilon_{sink} = \sum \frac{m}{2} \left(\sum_{Heat\ sink} v_{new}^2 - \sum_{Heat\ sink} v_{old}^2 \right) \tag{2.48}$$

From the calculated kinetic energy, the average energy changing is computed as following equation;

$$\Delta\varepsilon_{ave} = \frac{\Delta\varepsilon_{source} + \Delta\varepsilon_{sink}}{2} \tag{2.49}$$

From this equation, thermal conductivity is calculated as;

$$k = -\frac{J}{A(dT/dx)} = -\frac{\Delta\varepsilon_{ave}}{A\tau(dT/dx)} \quad (2.50)$$

In the above formula, $\Delta\varepsilon$ describes the change in average energy per unit time which is constant heat flux (J), τ describes the duration of time when the thermostats are active, and A defines the cross-sectional area of the simulation model to the heat flux direction. τ was chosen from four different values which is shown in Figure 2.14. τ was set as $50\ fs$ providing the best convergence around 300 K.
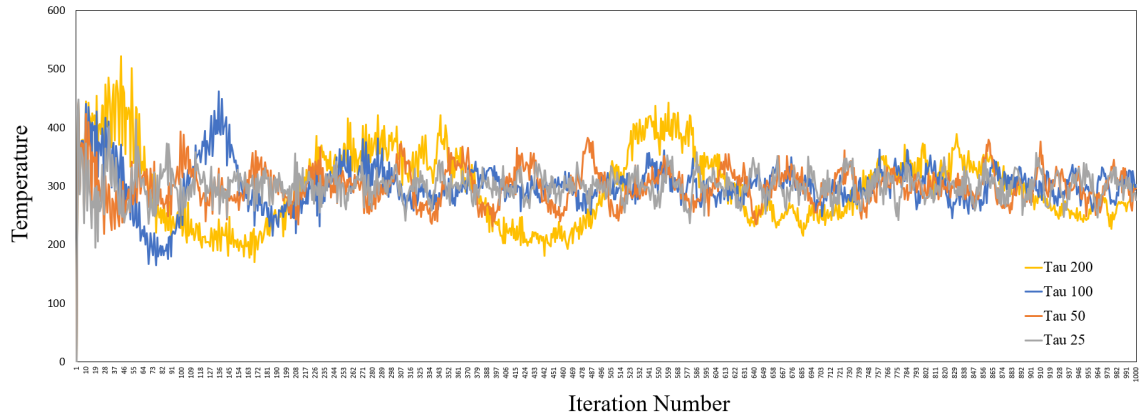
Figure 2.14. System temperature for different τ.

After the simulation time finalized, the linear regression method is used to obtain the temperature gradient dT/dx in the x-direction as following equations. The slope is calculated as a linear equation as $y = a_0 + a_1x$. a_1 gives the slope of the system (dT/dx) where y is temperature of the slab and x is the distance of the slab.

$$a_1 = \frac{n\sum_{i=1}^{n} x_i y_i - \sum_{i=1}^{n} x_i \sum_{i=1}^{n} y_i}{n\sum_{i=1}^{n} x_i^2 - \sum_{i=1}^{n} x_i} \quad (2.51)$$

$$a_0 = \frac{\sum_{i=1}^{n} x_i^2 \sum_{i=1}^{n} y_i - \sum_{i=1}^{n} x_i \sum_{i=1}^{n} x_i y_i}{n\sum_{i=1}^{n} x_i^2 - \left(\sum_{i=1}^{n} x_i\right)^2} \quad (2.52)$$

All simulations are performed with MPI (Message Passing Interface) algorithm to obtain less simulation time. MPI is a parallel algorithm which basically, supports a fast way to solve an algorithm by computing with more than one core and it shares calculated results by sending or receiving between the cores. Without using a parallel algorithm, computing gets more difficult. This cause increases the simulation time. Therefore, a parallel algorithm integrated into the code and running time reduced by choosing a core number according to the system size. Finally, the thermal conductivity of the system computed from the last 10×10^6 data. Figure 2.15 summarizes the MD.
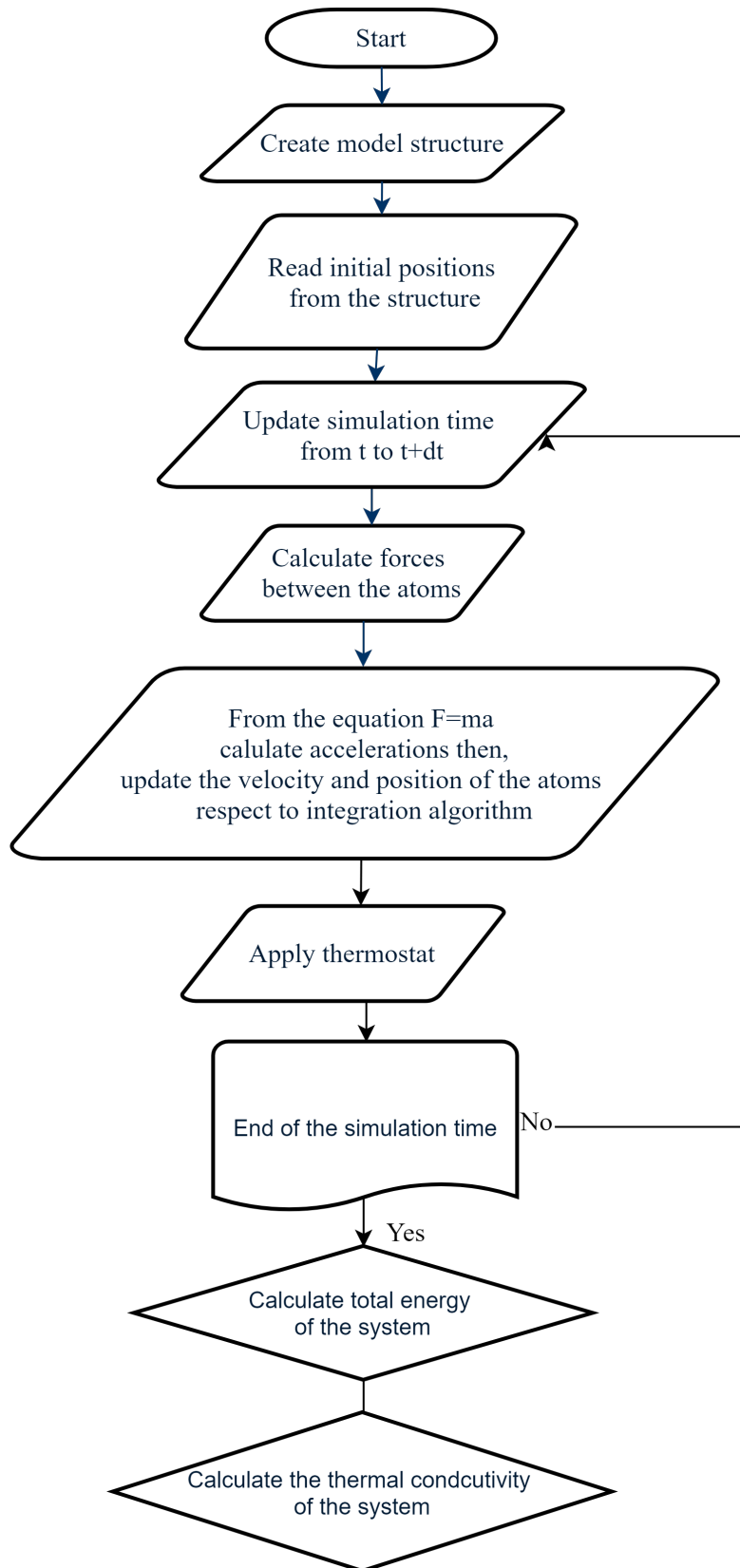
Figure 2.15. MD simulation flow chart.

2.3. Results and Discussion

The created NEMD simulation code is compared with the literature calculations. The results shows that the thermal conductivity results are in good agreement with the literature. Guo et al. (2009), Cao et al. (2012), and Wei et al. (2011) found the thermal conductivity of single-layer graphene using LAMMPS that has the similar dimension with our study which is close enough with our result. When the graphene thickness takes according to these studies 0.335 nm and 0.144 nm respectively, the thermal conductivity of single-layer graphene value finds as shown in Figure 2.16. When these studies compare, the results give good agreement with our MD results.
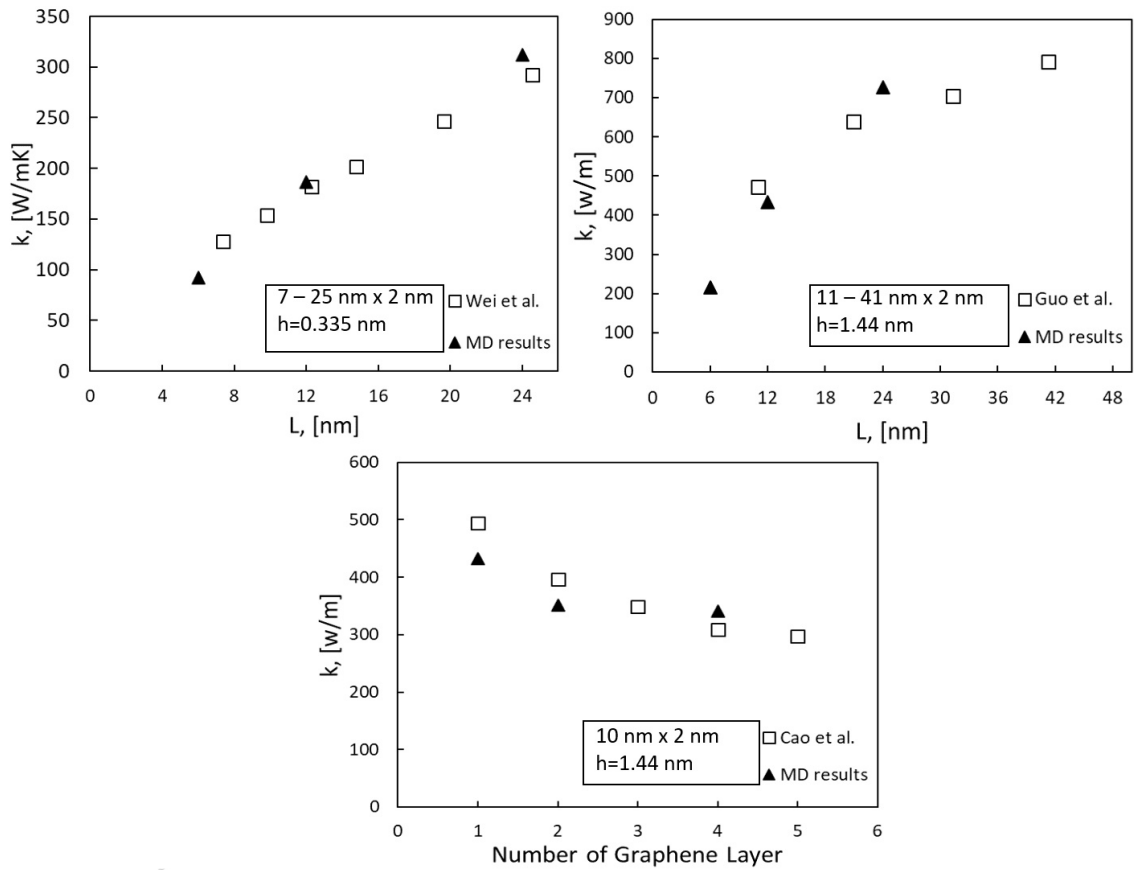
Figure 2.16. Thermal conductivity of single layer graphene comparison with different studies a) Wei et al take graphene thickness 0.335 nm, b) Guo et al and c) Cao et al. take graphene thickness 0.144 nm.

The thermal conductivity of SLG and MLG (2 layer and 4 layer graphene) plotted as a function of length ranging from 6 nm to 24 nm at 300 K as shown in Figure 2.17. The results show that the thermal conductivity of the SLG is higher than the MLG.
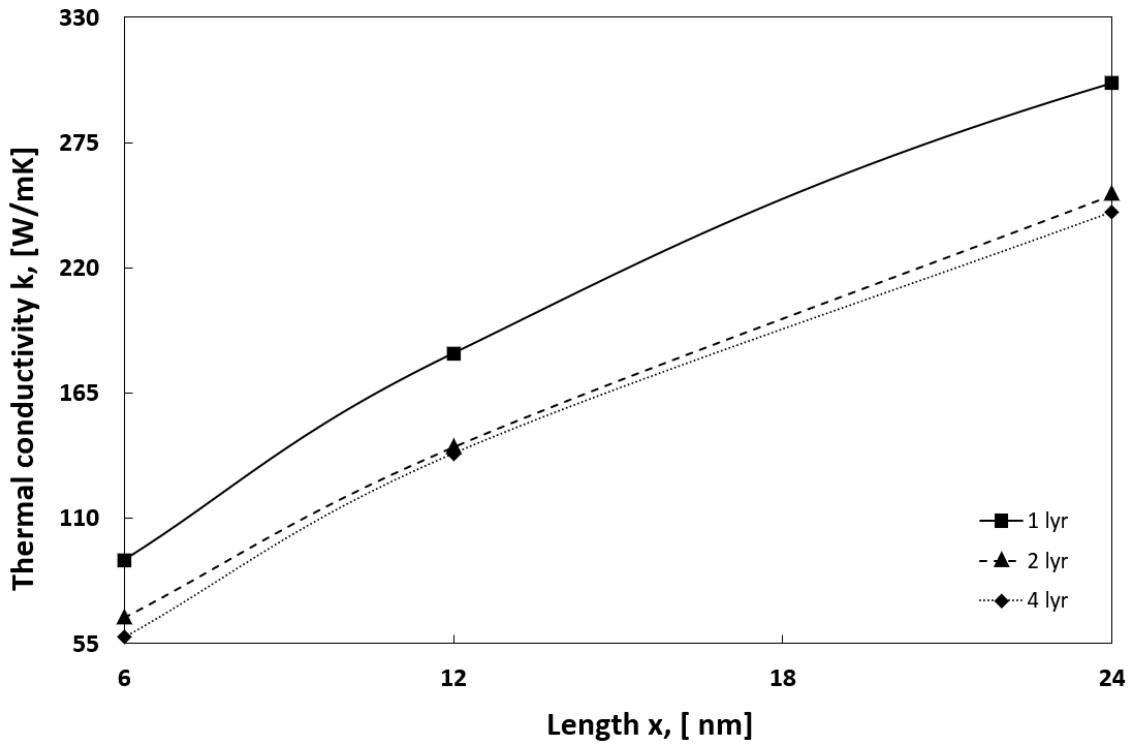
Figure 2.17. Thermal conductivity of graphene for different number of layers (width: 3 nm, height: 2 nm).

The thermal conductivity decreases with the number of graphene layers increase as it has been obtained in the literature (Nika and Balandin, 2016; Wei et al., 2011; Cao et al., 2012). Moreover, the neighboring layer creates an obstacle to phonon transport because it restricts the atom's movement. Thus, this demonstrates that the thermal conductivity of the SLG will be reduced when coated or the number of layers increased. As another outcome from these results is that the thermal conductivity changes with the length.

The magnitude of the founded thermal conductivity of the SLG is much lower to compare with the experimental values in the literature. The reason is that the heat conduction in graphene dominates by phonons and it is affected by the PMFP. When the length of graphene shorter than the PMFP then the thermal conductivity increases until to reach it. This shows that graphene has a strong size dependence. According to the power law which is $k \sim L^{\beta}$, the thermal conductivity can be predicted unknown length under the PMFP. β calculated by the least-squares fit method as 0.43 as shown in Figure 2.18, in the literature it varies from 0.3 to 0.49 (Guo et al., 2009; Zhu et al., 2017). In a similar way, the thermal conductivity of pure Cu and graphene-coated Cu models investigated. Figure 2.19 shows the thermal conductivity changing by the length dependence from 3 nm to 12

nm with the same width and height in Cu, SLG-Cu, and MLG-Cu models.
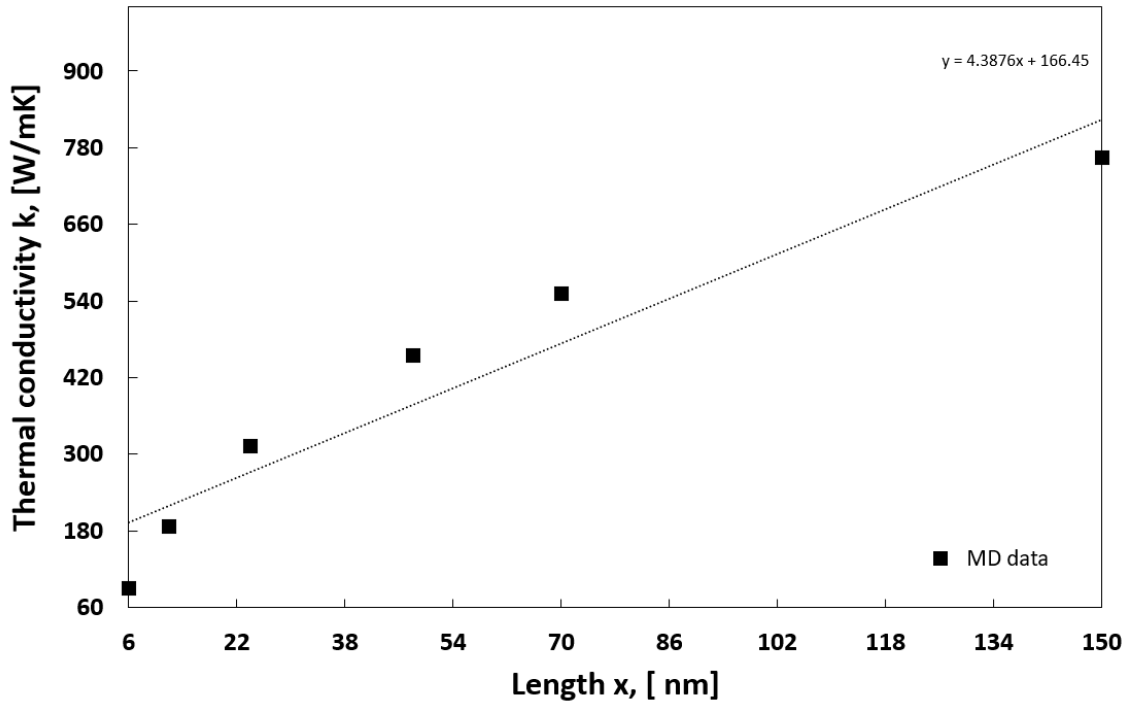
Figure 2.18. The thermal conductivity of single layer graphene linear curve prediction according to the power law.

Our results indicate that when the pure copper coated with SLG, the thermal conductivity of copper increases about average 18% and similarly coated with 2-layer graphene, the average increment at the thermal conductivity is obtained about 33% and finally coated with 4-layer graphene, the thermal conductivity changing increases about average 49% by the length changes.

According to this completed results, copper's thermal conductivity is founded max about 2.15 W/mK that is much smaller than the bulk copper's thermal conductivity which is 380 W/mK at 300 K (Jagannadham, 2012). This is because, in metal, heat is carried out with phonons, and electrons but, classical MD simulations of metals underestimate the magnitude of the thermal conductivity due to lack of free electron contribution. More-over, it is demonstrated that electron contribution on the total thermal conductivity of copper dominates about 95% whereas the phonon contribution is effected on the thermal conductivity about 5% at 200 K. (Momenzadeh et al., 2013).

In addition, it can be said when the materials like copper coated with graphene, the interactions and phonon scattering between them cause to reduce the PMFP. Thus, the thermal conductivity of the graphene-coated system converges at a smaller value of

PMFP, than graphene's PMFP. However, the convergence of the thermal conductivity cannot be seen due to the simulation model size is too large. Moreover, phonon contribution effect on the thermal conductivity decreases gradually as temperature increases. When the temperature increases that induces a problem with movement of atoms which leads phonon scattering. Hence, thermal conductivity reduces. Figure 2.20 demonstrates the temperature effect on thermal conductivity in Cu and SLG-Cu models.
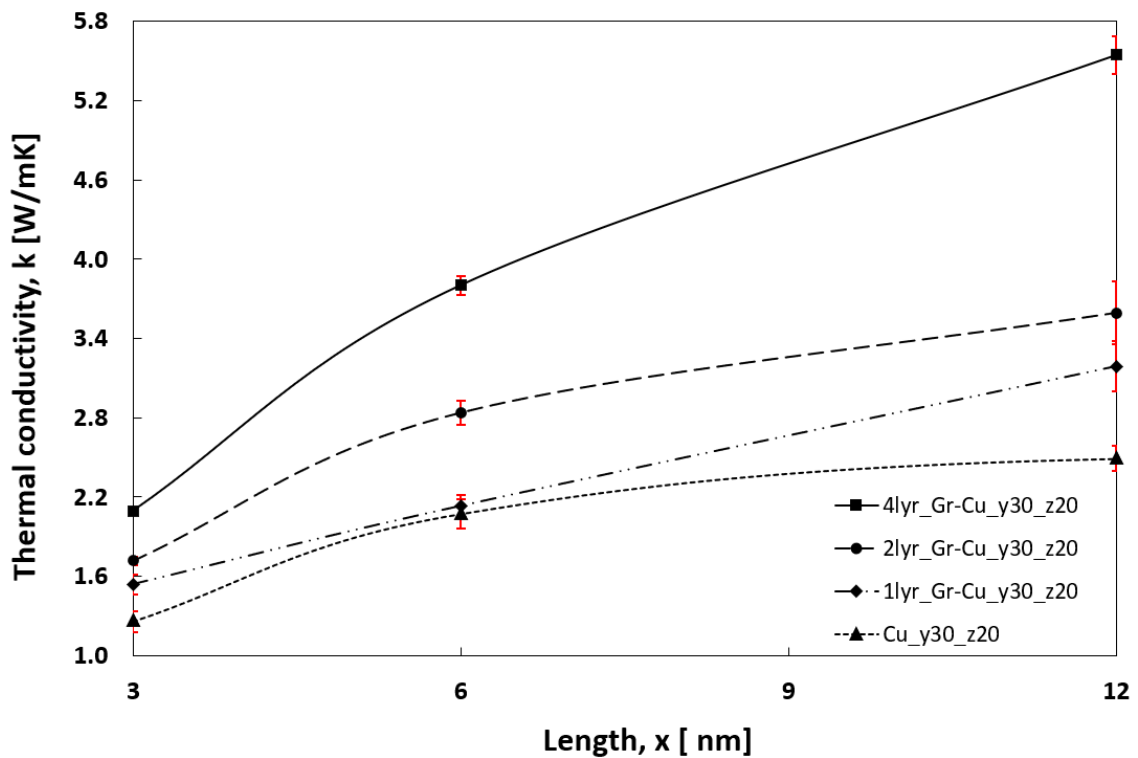
Figure 2.19. Thermal conductivity of Cu, SLG-Cu, and MLG-Cu for varies lengths
            (width: 3 nm and height: 2 nm).

Researchers have generally investigated the thermal interface between graphene and metal system so that, our results couldn't be validated with other results for SLG-Cu and MLG-Cu systems. Though Zhu et al. (2017) studied thermal conductivity of SLG coated Ni by using MD and they found that thermal conductivity increases with length in plane direction. Besides, Goli et al. (2014) experimentally demonstrated that the thermal conductivity of graphene coated copper increases compared to pure copper. They also studied the thermal conductivity of MLG-Cu. Their results give higher values than SLG-Cu so that, they interpreted this behavior as a grain size effect.

Figure 2.21 shows the width effect on thermal conductivity from 1.5 nm to 6 nm. It indicated that the thermal conductivity increases with the width increases. This is because, the boundary scattering and edge localized phonon effect gets weaker when the

width increases. Therefore the resistance in the samples gets reduce.
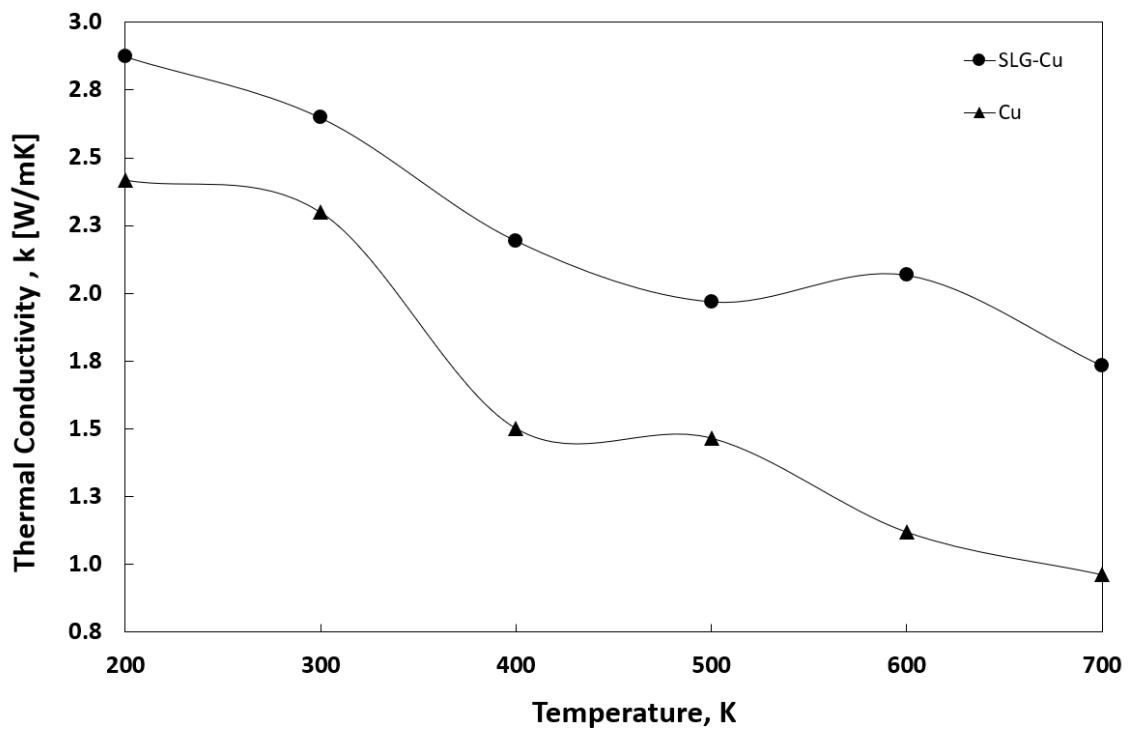
Figure 2.20. Temperature effect on the thermal conductivity of copper and graphene-
coated copper model.

Our results present that when the pure copper coated with SLG, the thermal con-
ductivity of copper increases about average 12% likewise coated with 2-layer graphene,
the average increment at the thermal conductivity is obtained about average 28% and
coated with 4-layer graphene the thermal conductivity changing increases about average
44% by width changing. Therefore, it can be said that length dependence on the ther-
mal conductivity in-plane direction is much more affected than the width because of the
graphene long PMFP.

As it can be observed from Figure 2.22 when the copper coated with SLG the
thermal conductivity increases about average 6%, in the same way, coated with 2-layer
graphene, the average increment on the thermal conductivity is obtained about average
21% and coated with 4-layer graphene the thermal conductivity changing increases about
average 37% by height changing. It is noticeable that increasing the height isn't affected
the thermal conductivity that much compared to length and width.

Figure 2.21. Thermal conductivity of Cu, SLG-Cu, and MLG-Cu for varies widths (length: 6 nm and height: 2 nm).

Figure 2.22. Thermal conductivity of Cu, SLG-Cu, and MLG-Cu for varies heights (length: 6 nm and width: 3 nm).

2.4. Conclusion

The thermal conductivity of pure copper, graphene models (SLG and MLG) and graphene-coated copper models (SLG-Cu, MLG-Cu) investigated using o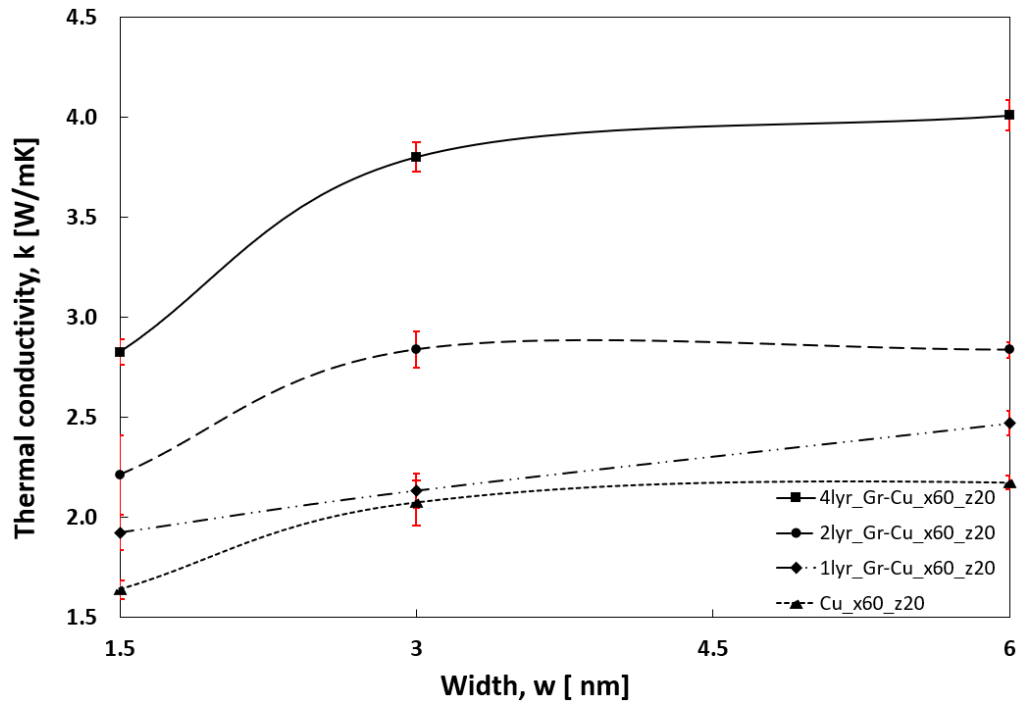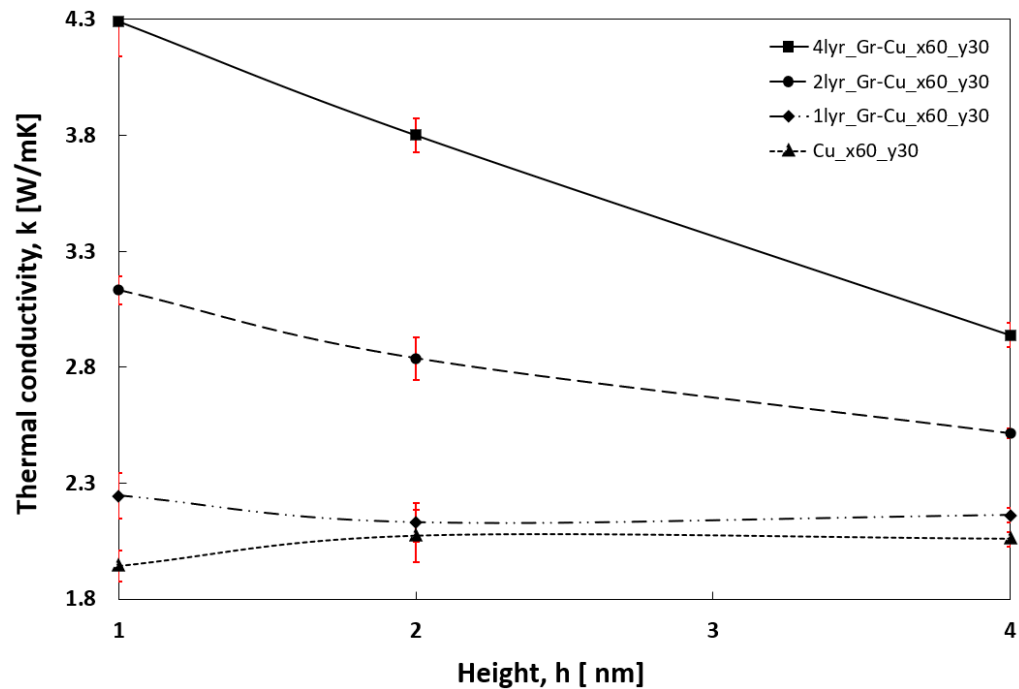ur MD code. The thermal conductivity of the simulation model is studied with different length, width, and height to see their effect. The results indicated that the thermal conductivity increases with length. This phenomenon can be explained as following; length dependence is an important factor for the low-dimensional systems and long PMFP causes a strong length dependence. Further, when the width increases then the thermal conductivity also increases because of reducing the boundary scattering effect. In addition, increasing height didn't affect the thermal conductivity as much as length and width. Still, the thermal conductivity increases when the height will increase.

Another outcome is that phonon contribution effect on the thermal conductivity decreases when the temperature increases. Temperature increment causes a problem with the movement of atoms which leads phonon scattering. Thus, thermal conductivity reduces. Our findings support that the thermal conductivity of graphene coated model is higher than the uncoated ones. Furthermore, results also indicate that single layer graphene (SLG) model has the highest thermal conductivity as compared to the other model. However, when graphene is bonded or coated with other materials, the strength between neighboring layers causes reduces the thermal conductivity.

Consequently, this study show that the thermal conductivity of copper is improved by coating graphene that has high thermal conductivity.

CHAPTER 3

THERMAL PERFORMANCE INVESTIGATION OF GRAPHENE-COATED COPPER

This chapter investigates the thermal performance of graphene coated copper foil experimentally. Thermal performance of pure copper, annealed copper, and multi-layer graphene coated copper foil was tested with different volume flow rate and based temperature. It was observed that coating with graphene enhanced the heat removal performance of copper foil.

3.1. Methodology

In this section, it was provided about the experimental set-up and properties of the samples.

3.1.1. Preparation of samples and sample holder

In this work, the graphene film was obtained by chemical vapor deposition (CVD) on copper foil and supplied from Quantum Device Laboratory in IZTECH. The sample size are $50\ mm$ x $25\ mm$ and $20\ mm$ x $25\ mm$ with $25\ \mu$m thickness. Figure 3.1 shows the SEM images of bare, annealed and graphene grown Cu foils are shown in Figure 4(a), 4(b) and 4(c), respectively.
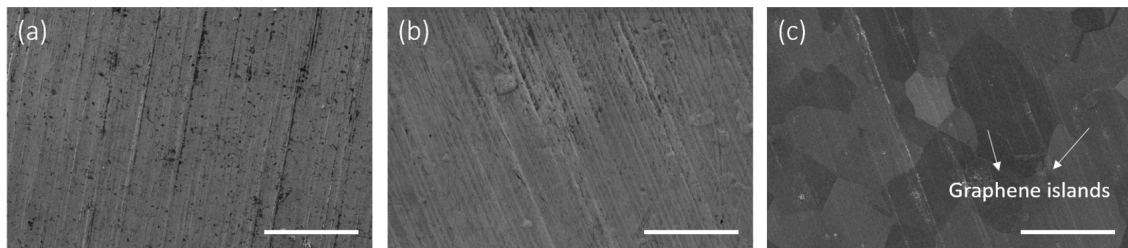
Figure 3.1. SEM images of (a) bare, (b) annealed (before graphene growth) and (c) graphene grown Cu foils.

The samples of graphene coated on copper, pure copper and annealed copper with two different size are shown in Figure 3.2.
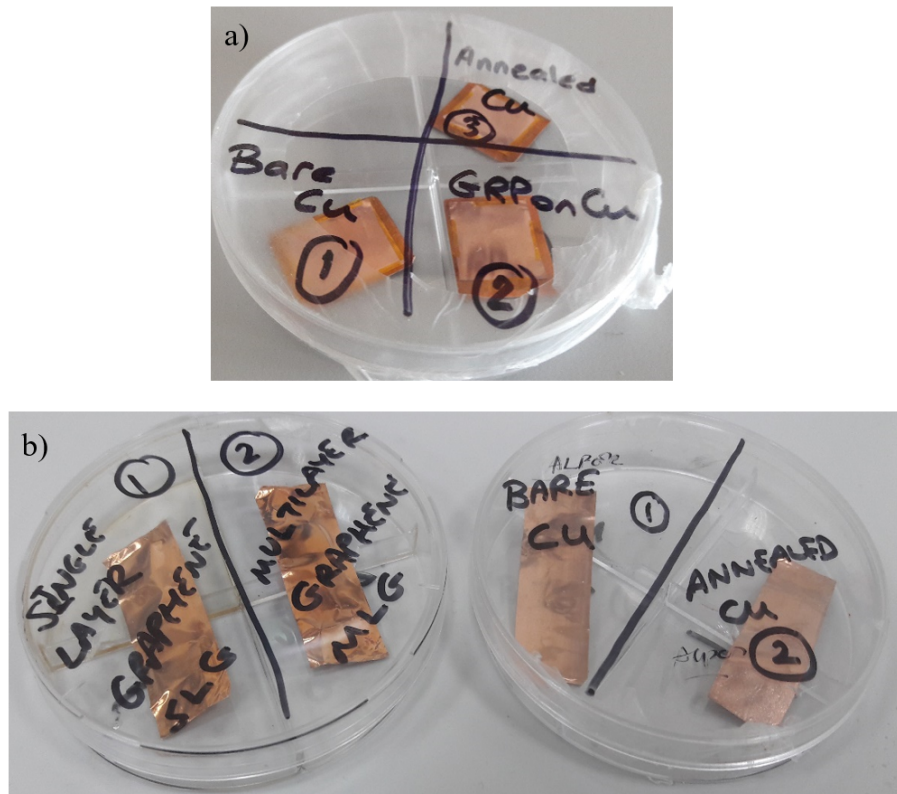
Figure 3.2. The samples with the size of a) 20 mm x 25 mm, b) 50 mm x 25 mm.

A sample holder device was designed to hold the fabricated graphene on Cu foil and place thermocouples and heating device. $10\ mm$ (bottom holder) and $3\ mm$ (top cover) polycarbonate plate was used to form the sample holder. They were designed with CAD programming according to the two different sample size. The poly-carbonate plate has a $115\ mm$ x $55\ mm$ ($85\ mm$ x 55 mm) rectangular shape. Figure 3.3, Figure 3.4, Figure 3.5, and Figure 3.6 shows the dimension of sample holder and cap of it.

In the middle of the plate for the sample placement there is a rectangle shape with a $4\ mm$ depth recess is created in the bottom plate to hold the manufactured samples. A rectangle channel with $1\ mm$ depth from the surface was created around the $4\ mm$ depth recess to protect samples from the water directly and samples are located under this in the recess.

Figure 3.3. 3D design of sample holder with the size of 5 cm x 2.5 cm a) 3D view, b) Front view, c) Left view, d) Top view.

a)

b)

c)

d)

3 mm

55 mm

1 mm

4 mm

4 mm

5.50 mm

3 mm

115 mm

4 mm

5.50 mm

95 mm

87 mm

27 mm

35 mm

55 mm

Figure 3.4. 3D design of cap of sample holder with the size of 5 cm x 2.5 cm a) 3D view, b) Front view, c) Left view, d) Top view.

Figure 3.5. 3D design of sample holder with the size of 2 cm x 2.5 cm a) Left view, b) Top view, c) Front view, d) 3D view.
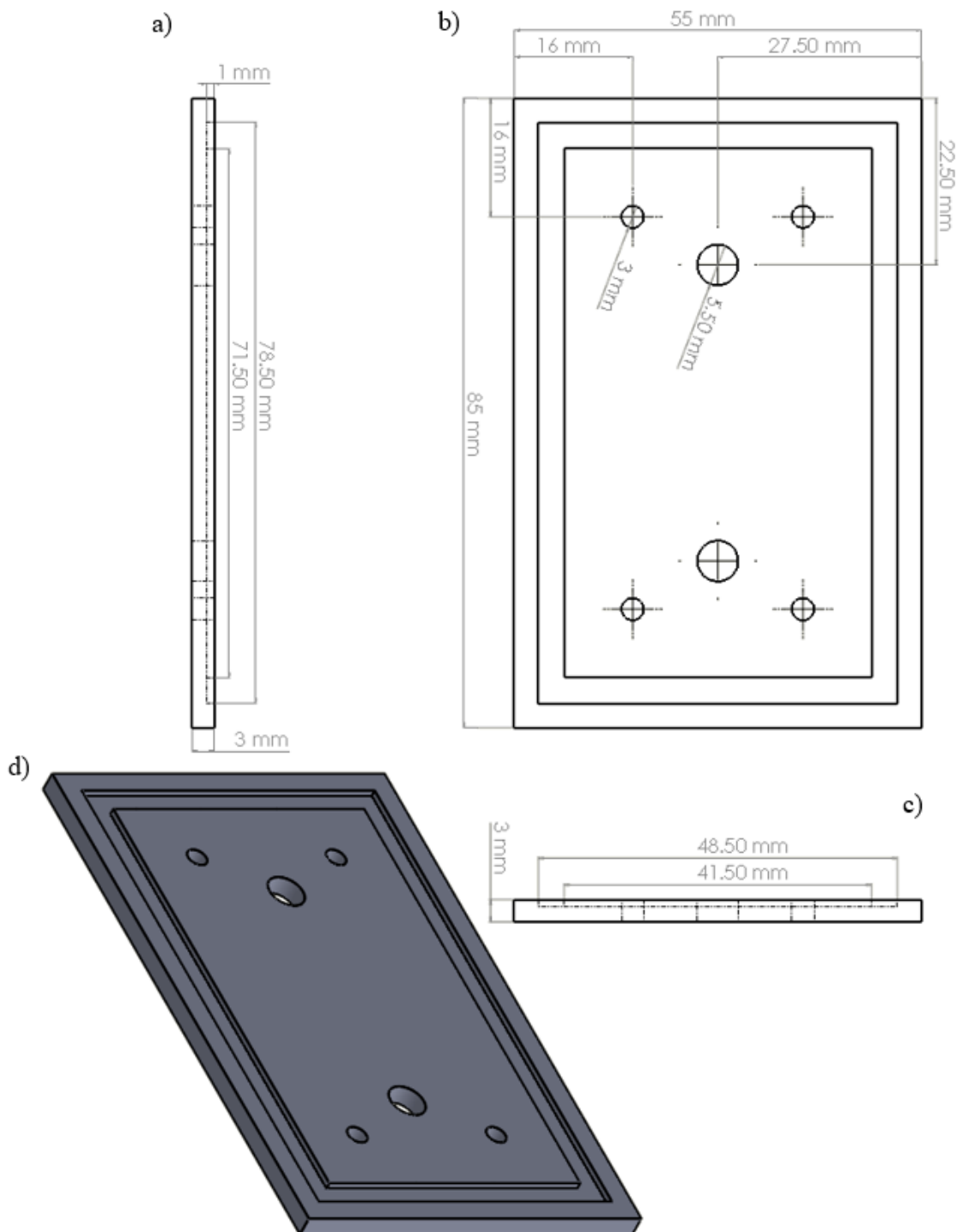
Figure 3.6. 3D design of cap of sample holder with the size of 2 cm x 2.5 cm a) Left view, b) Top view, c) Front view, d) 3D view.

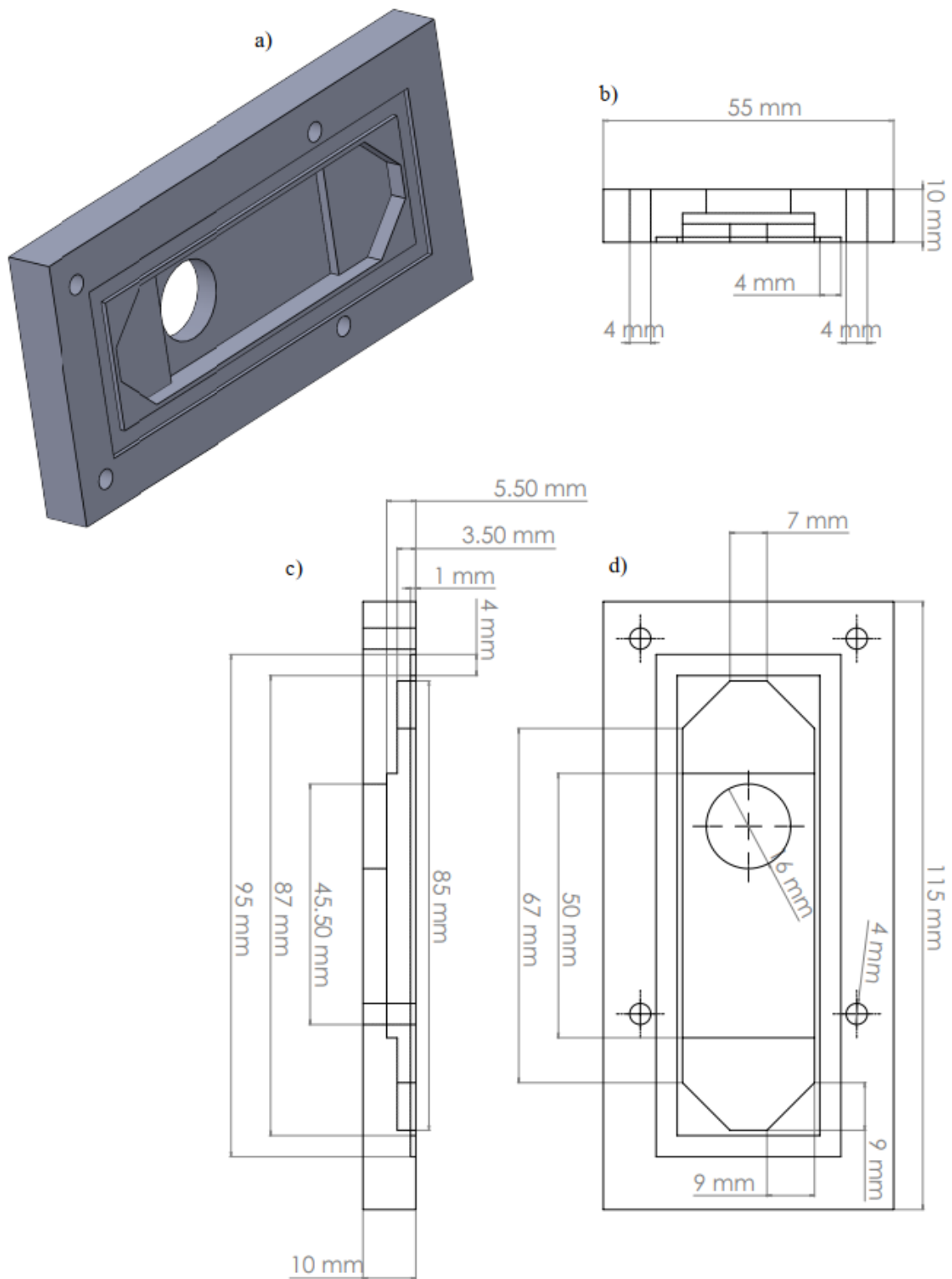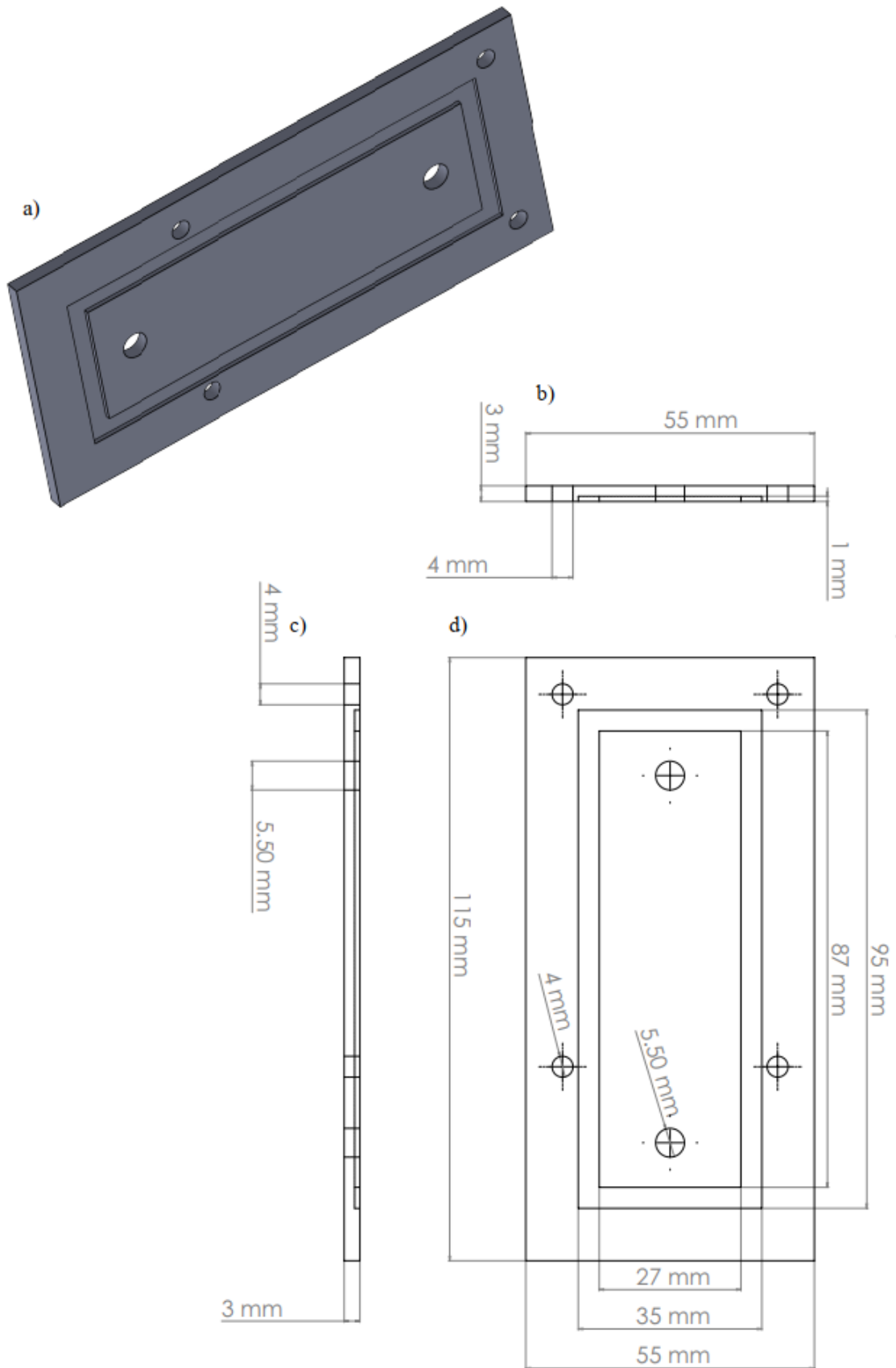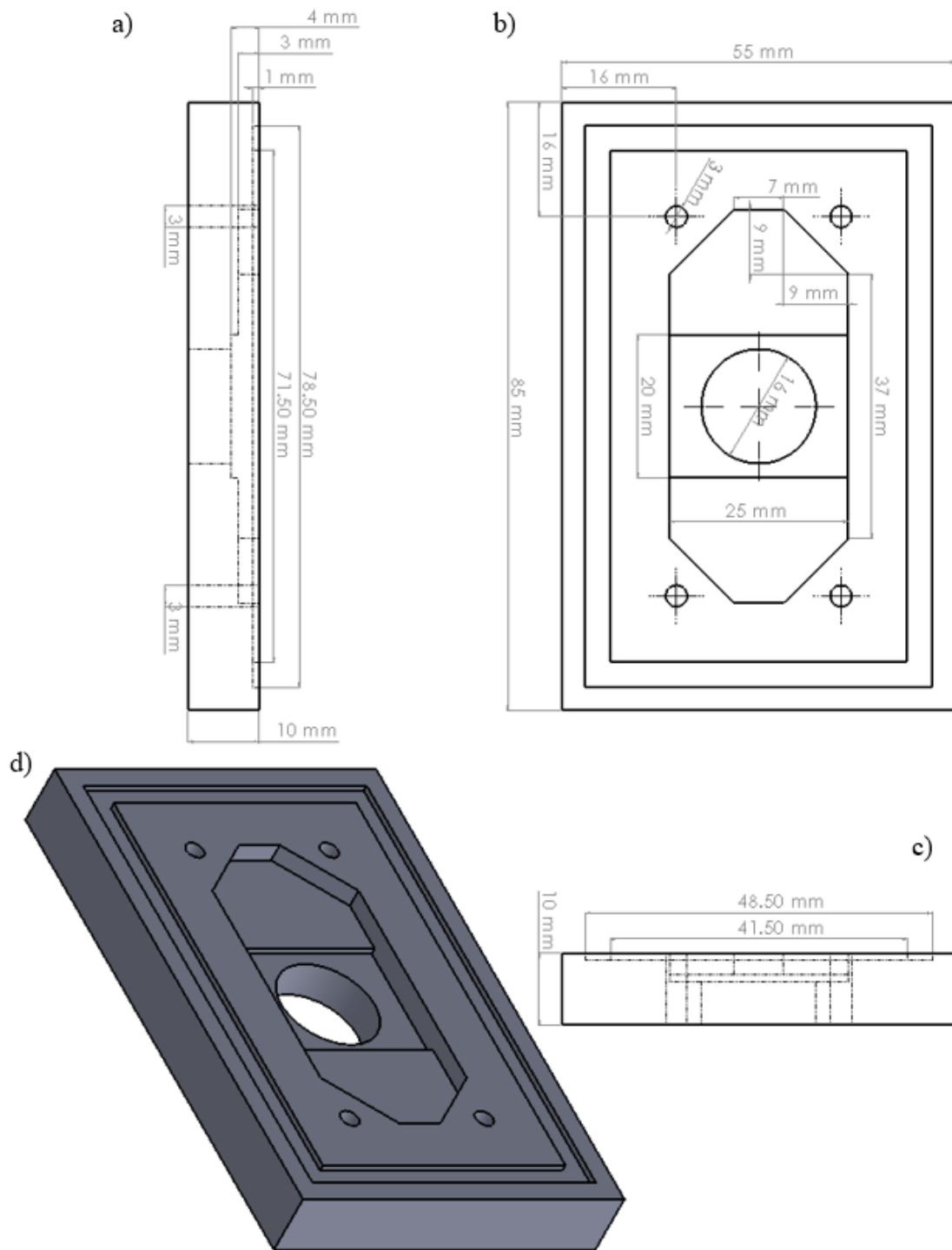The copper block that has 16 mm diameter and 84 mm length is placed under the right end of the recess to obtain the heat dissipation of the sample from through right to left. Three holes are drilled into the copper block to measure the temperature with using K type thermocouple. Moreover, four holes were drilled, and thermocouples were fixed into the polycarbonate plate to observe the heat dissipation in the sample. All thermocouples were fixed by silicone gasket into their places. Furthermore, the foam cloth as insulation was used around the copper block and the sample holder to prevent heat loss. Figure 3.7 shows the schematic diagram of the sample holder.
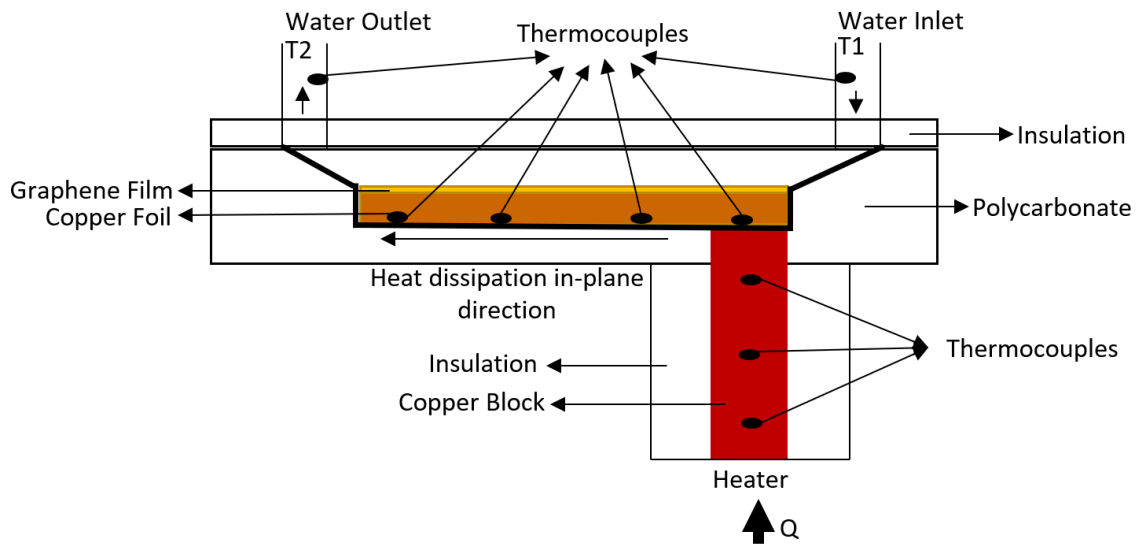
Figure 3.7. Schematic diagram of the sample holder.

In addition, PID controlled heater was used to turn up and down the heat as the desired temperature. The sample holder was placed to the copper block to hold the system at desire-based temperature via the heater. Then, the samples were located in the recess to touch the copper block. A thin layer thermal interface material is applied which has over than 1.93 W/mK thermal conductivity value, to obtain good thermal contact between the copper block and the sample. The experimental set-up has been starting after the sample holder designed. As indicates in Figure 3.8 the following steps presents the sample holder combine procedure.

a. Firstly, sample holder was placed to the copper block to hold the system desired based temperature.
b. Samples were located the copper block as to touch it.
c. Resistance heater was coupled with the copper block.
d. A wooden block was designed to prevent heat loss and also to provide balance to the sample holder.

45
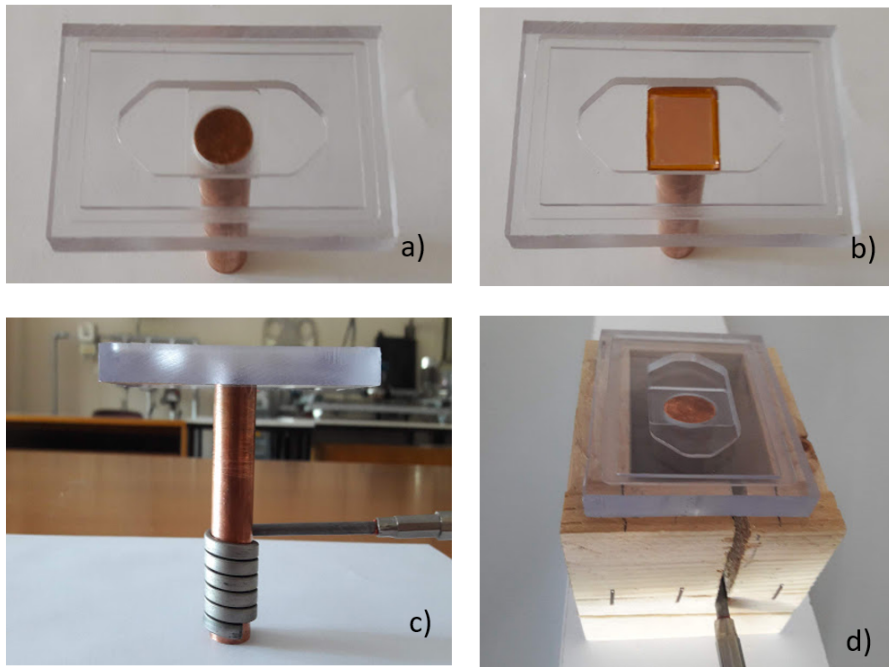
Figure 3.8. Designed sample holder combine procedure.
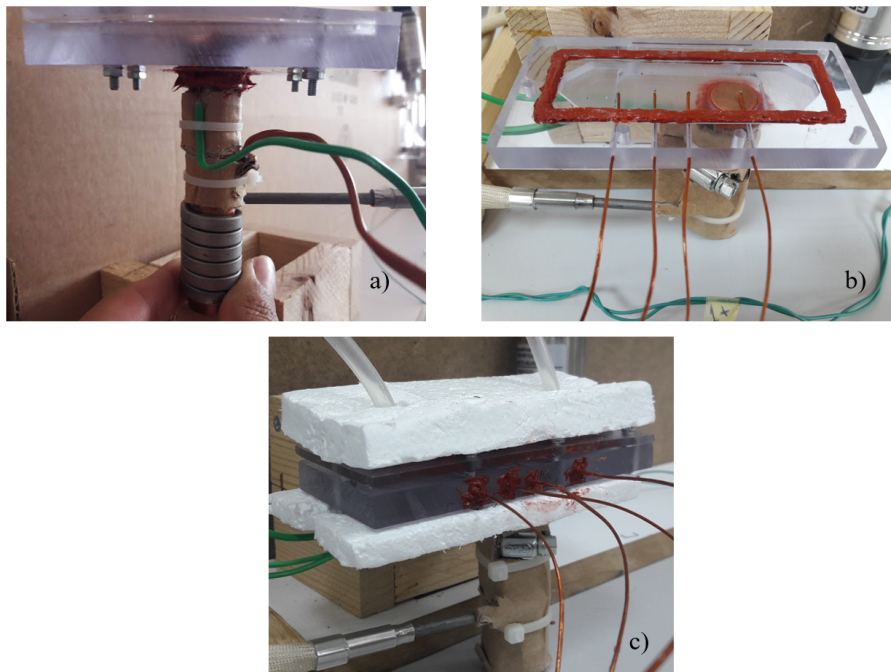
Figure 3.9. Places of thermocouples on the sample holder a) in copper block and b) in polycarbonate plate. c) The last form of sample holder.

After these steps, the designed sample holder is shown in detail in Figure 3.9. In the figure below (a) shows the location of the thermocouple in the copper block. The bottom one belongs to the heater, while the other two of them to observe the temperature by the desired value. (b) shows location of the thermocouple where sample locate to observe the heat dissipation in the sample. and (c) shows the last form of sample holder with foam cloth insulation before the experiment.

3.1.2. Uncertainty Analysis of Thermocouples

A water-bath device which is set the water temperature was used to check the uncertainty of the temperature measuring of thermocouples to be used in the experiment.

ii) Adjusting the water bath the desired temperature

i) The maximum temperature set for water temperature

on / off switch
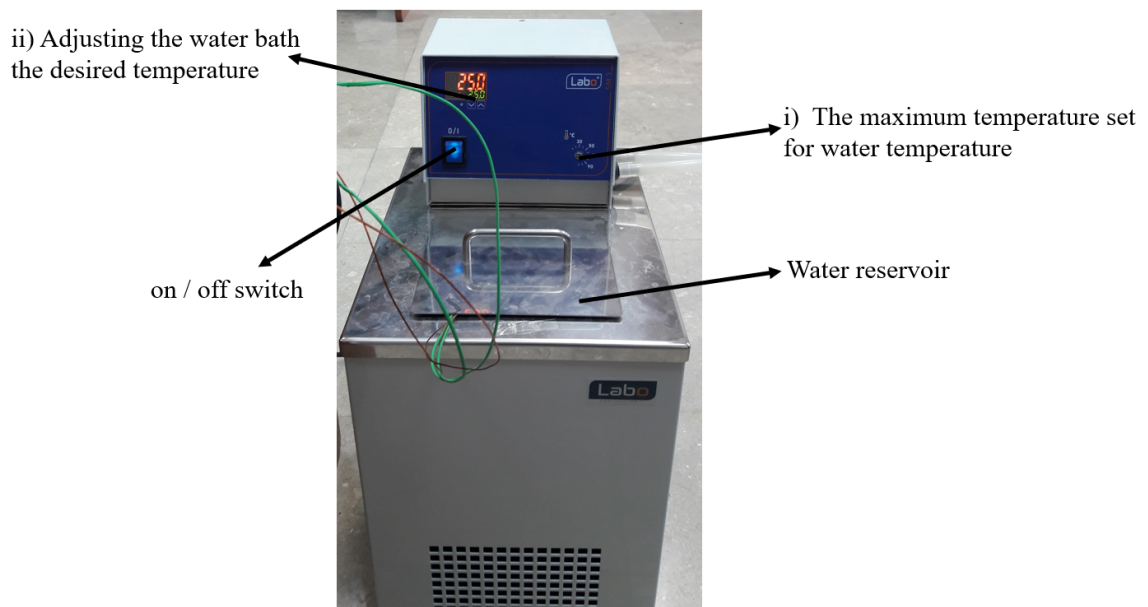
Water reservoir

Figure 3.10. Water-bath device.

The following steps were followed in the use of the water bath device which is shown in 3.10.

1. The water remaining in the reservoir of the water bath was drained from the drain valve at the back of the device.
2. Then the pure water was added to inside the reservoir until covering the top of the heating pipes.
3. The temperature of the water bath was brought to the highest measurement temperature which is highest temperature to be tested, with the instrument switched on as shown in Figure 3.10.(i)

47

4. As shown in Figure 3.10.(ii), after the water bath is brought to the desired temperature, it is checked that the water bath works correctly at the desired temperature with the help of a thermometer as shown in Figure 3.11(a).

5. To check the uncertainty of the temperature measurements, the thermocouples were placed in the reservoir of the water bath as shown in 3.11(b).

6. The values measured by the thermocouples were obtained by increasing and reducing the temperature of the water bath as shown in Figure 3.12.
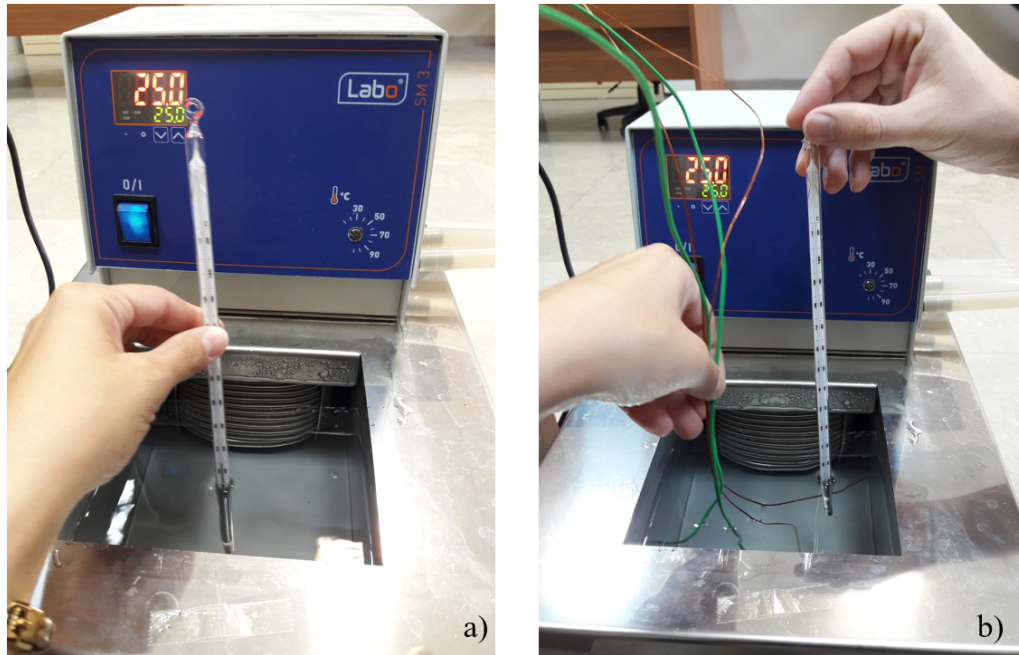
Figure 3.11. Testing of Water-bath a) Control of Water-bath temperature by thermometer b) Placing thermocouples in water bath device to check the uncertainty of temperature measurements.

The water bath was first set to 25^oC, Increasing by 5^oC, the temperature increasing up to 80^oC, and reducing by 10^oC, starting from 75^oC to 35^oC. Temperature measurement values of thermocouples were found as linear when heating and cooling the water as expected which shown in Figure 3.12.

Termocupl hysterisis problem is controlled by thermometer and termocupl using water-bath device while water was heating and then cooling. It was observed that there is no hysterisis problem with thermocuples. Also, it was measured that uncertainties for thermocouples about $0.1^\circ C$
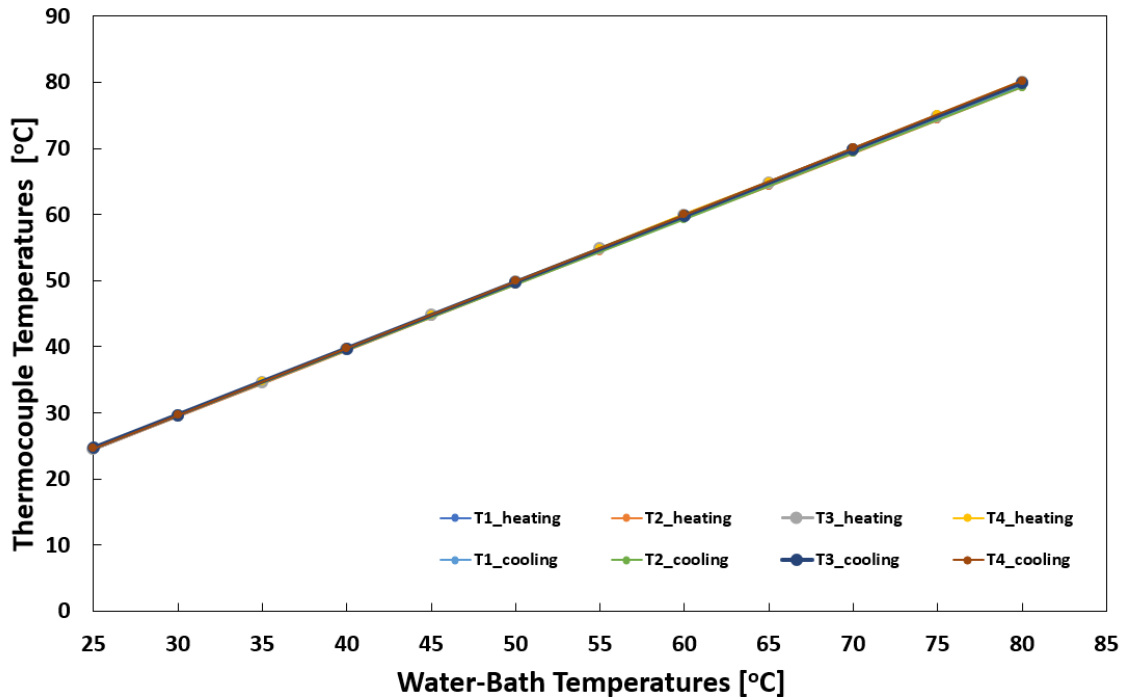
Figure 3.12. Temperatures measurement of thermocouples at set water bath temperature (heating/cooling).

3.1.3. Experimental Set-up

The experimental set-up is prepared to test thermal performance of graphene coated copper foil with different volume flow rates which are $50\ ml/dk$, $75\ ml/dk$, and $100\ ml/dk$ and different based temperatures as $40°C$, $60°C$, and $80°C$. Figure 3.13 shows the schematic diagram of experimental set-up flow loop. The experiments are led done for 30 minutes at setting volume flow rate changing the based temperature from $40°C$ to $80°C$. Then, the results are taken for the last 10 minutes after the system become steady-state.

The experimental set-up is shown in Figure 3.14 by describing the following steps.

1. When the test starts, firstly, de-ionized water was pumped through using LeadFluid peristaltic pump. The pump consists of a pump head according to using silicone hose pipe diameter in the experimental set-up and a self-control flow rate system.
2. After, pumped water passes through the pulsation dampener to discard the peristaltic effect of the pump and also unwanted air-gap.
3. Then, float glass tube flow meter was used to compare the the volumetric flow rate value reading from the pump.
4. After that, unwanted pressure and likewise air-gaps was eliminated inside the hose pipe via the toggle valve.

49
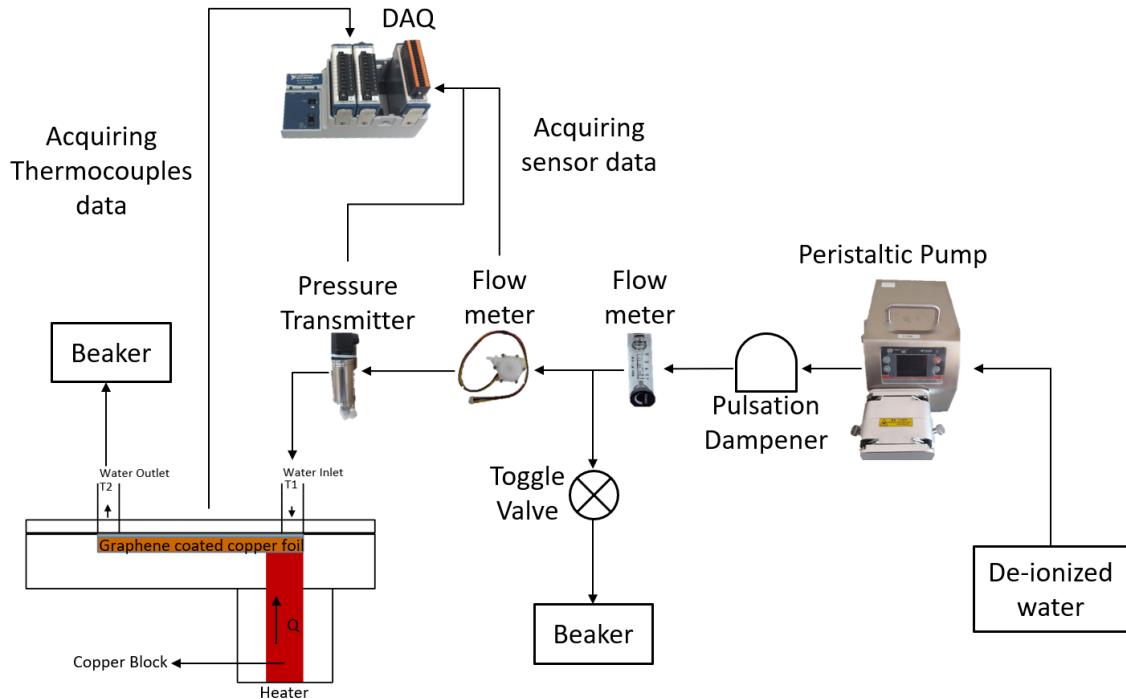
Figure 3.13. Schematic diagram of experimental set-up flow loop.

5. Stable and non-air gap water's volume flow rate was checked using PVC turbine flow meter for the second time.

6. Next, water's inlet pressure was read by National Instruments CompactDAQ data acquisition system (DAQ). There is one pressure transmitter was used to measure the inlet water pressure since this system is an open loop which ending with atmospheric pressure.

7. Additionally, the data from seven thermocouples, which were located four of them to sample and three of them in the copper block were read from the DAQ.
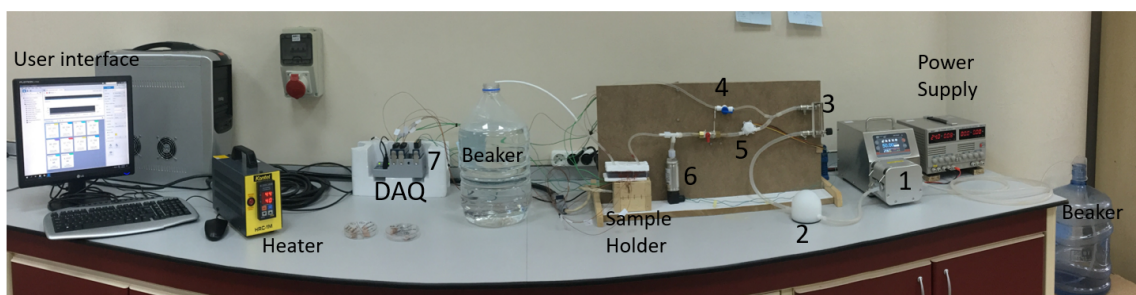
Figure 3.14. Experimental set-up.

After that, the results are obtained, the heat flux is calculated using Fourier law which is given below from the thermocouples measuring on the copper block.

$$q = k\frac{\Delta T}{\Delta x} \qquad \left[\text{W/m}^2\right] \tag{3.1}$$

Δx is the distance between thermocouples, ΔT is the differences between the thermocouples temperatures and k is the thermal conductivity of the copper block which is taken $385\ W/mK$.

3.2. Results and Discussion

According to the experimental results, the applied heat fluxes (q) to the copper block is given in Table 3.1 as an average value which depends on three different volumetric flow rates and based temperatures. It can be clearly said that from the table, heat fluxes get a higher value when the based temperature and volume flow rates increase.

Table 3.1. Experimental results of heat flux on the copper block to the three different sample depend on base temperature and volume flow rate.

|	Temperature (ºC)	Flow Rate (ml/min)	q (W/cm²)		Temperature (ºC)	Flow Rate (ml/min)	q (W/cm²)
Multi layer graphene coated copper foil	40		1.409	**Annealed copper foil**	40		1.581
	60	50	2.868		60	50	3.255
	80		4.636		80		5.971
	40		1.497		40		1.786
	60	75	3.079		60	75	3.617
	80		4.815		80		6.212
	40		1.673		40		1.883
	60	100	3.237		60	100	4.155
	80		4.838		80		6.387
	Temperature (ºC)	Flow Rate (ml/min)	q (W/cm²)		Temperature (ºC)	Flow Rate (ml/min)	q (W/cm²)
Copper foil	40		1.682	**Single layer graphene coated copper foil**	40		1.348
	60	50	4.309		60	50	2.946
	80		7.628		80		4.267
	40		2.034		40		1.537
	60	75	4.606		60	75	3.217
	80		7.802		80		4.542
	40		2.254		40		1.764
	60	100	5.155		60	100	3.361
	80		8.323		80		4.763

Figure 3.15 shows graphically the applied heat fluxes to the samples (MLG-Cu, An-Cu, and Cu) depend on based temperature. As can be seen from the figure, at the high-volume flow rate requires high heat transfer which means high heat flux necessity

to keep the temperature of samples near the based temperature. In through plane direction, un-coated samples transfer heat to the water directly according to coated ones. Thus, un-coated ones pull higher heat flux from the heater to keep system near the based temperature.
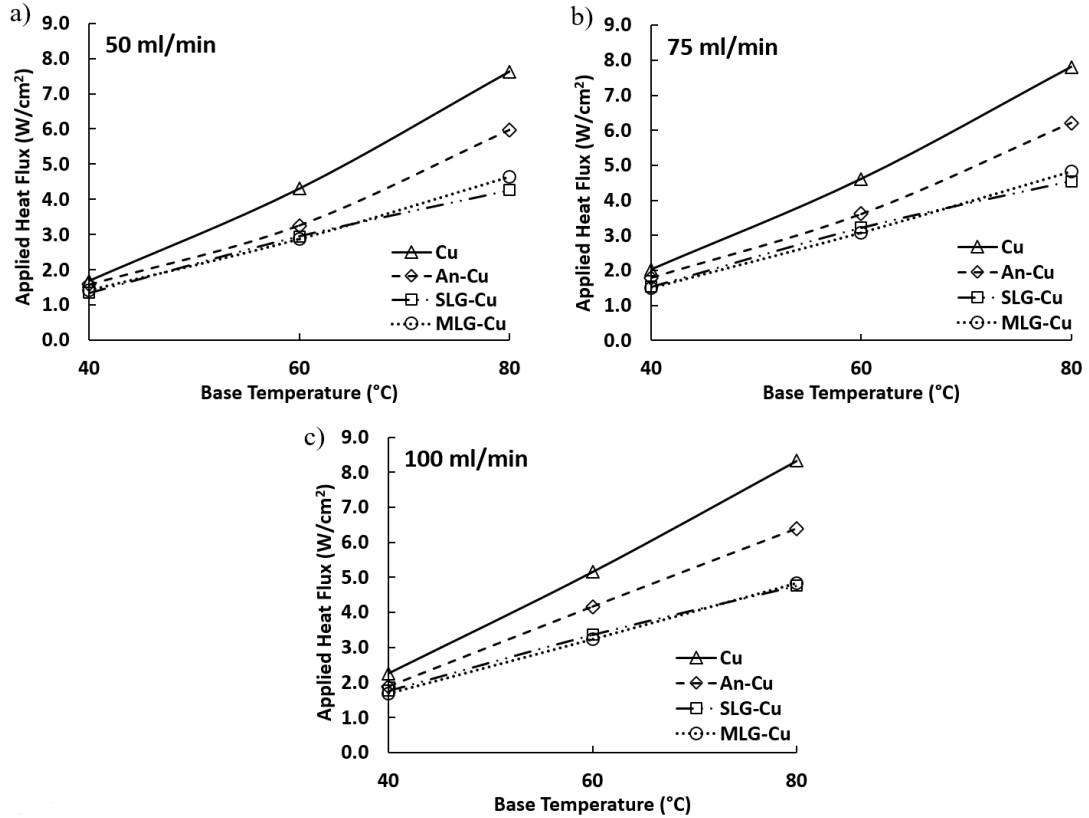
Figure 3.15. Applied heat flux to the copper block for the different base temperatures and volume flow rates on the samples a) 50 ml/min, b) 75 ml/min and, c) 100 ml/min.

At the same volume flow rate and based temperature, graphene-coated samples transfers heat to the water lower because of graphene's heat transport direction weak in through plane direction. Therefore, applied heat fluxes to them requires less energy transfer. Between the graphene-coated samples, the heat flux that applied to the SLG-Cu and MLG-Cu very close to each other. However, it was seen clearly at $80°C$ for all flow rates, SLG-Cu has a lower heat flux than the MLG-Cu. This means, for the same base temperature for all flow rates, graphene coated samples required less energy than the un-coated ones.

The average values of maximum temperature rising at the samples and the temperature differences of water between outlet and inlet is demonstrated in Table 3.2. The temperature rising in MLG-Cu and SLG-Cu samples have smaller value compared to un-

coated ones since graphene conduct heat immediately from the copper foil. Therefore, the maximum temperature of the coated samples it was observed less increment compare to others.

Table 3.2. Measuring maximum temperature rising of the samples and temperature differences of water between outlet and inlet.

	Temp. [°C]	Flow Rate (ml/min)	Water Temp. Diff. [°C]	Max. Temp. Rising [°C]		Temp. [oC]	Flow rate (ml/min)	Water Temp diff [°C]	Max. Temp. Rising [°C]
Multi layer graphene coated copper	40	50	0.9092	29.6188	**Annealed copper**	40	50	0.8950	31.0873
	60		1.6253	38.2702		60		2.2054	41.1814
	80		2.2358	46.0259		80		3.2760	48.1836
	40	75	0.2842	28.0352		40	75	0.6995	30.2963
	60		1.0638	35.8927		60		1.2125	37.0017
	80		1.7255	41.4744		80		2.3149	50.5028
	40	100	0.5217	27.6313		40	100	0.4669	28.4898
	60		0.9311	34.7610		60		1.1073	35.6042
	80		1.3116	39.4862		80		1.7634	47.0271

	Temp. [°C]	Flow rate (ml/min)	Water Temp. Diff. [°C]	Max. Temp. Rising [°C]
Copper	40	50	1.1372	31.2858
	60		2.6089	41.0630
	80		4.1944	52.6638
	40	75	0.7370	30.4198
	60		1.6397	37.7331
	80		2.8708	50.6032
	40	100	0.6222	28.7672
	60		1.3058	36.3950
	80		2.3097	47.7291

Furthermore, it is found that when the fluid flow rate is increased, the maximum temperature rising decreases. In addition, it was expected to increase water temperature, when the heater gives to the system higher heat fluxes. Hence, at the higher system temperatures, the water inlet temperature is increased as well as the outlet temperature.

Figure 3.16 indicates the temperature differences between water inlet and outlet depending on the applied heat fluxes. It can be clearly seen from the figure, for all flow rates, at coated graphene sample (MLG-Cu and SLG-Cu), the temperature differences between water outlet and inlet have smaller value compared to the others. It is because, at the graphene-coated copper foil, heat is passed through to the water fewer due to the conduction direction of graphene.

In other words, the temperature difference between water outlet and inlet is lower since the graphene conducts the heat in-plane direction immediately from the copper.
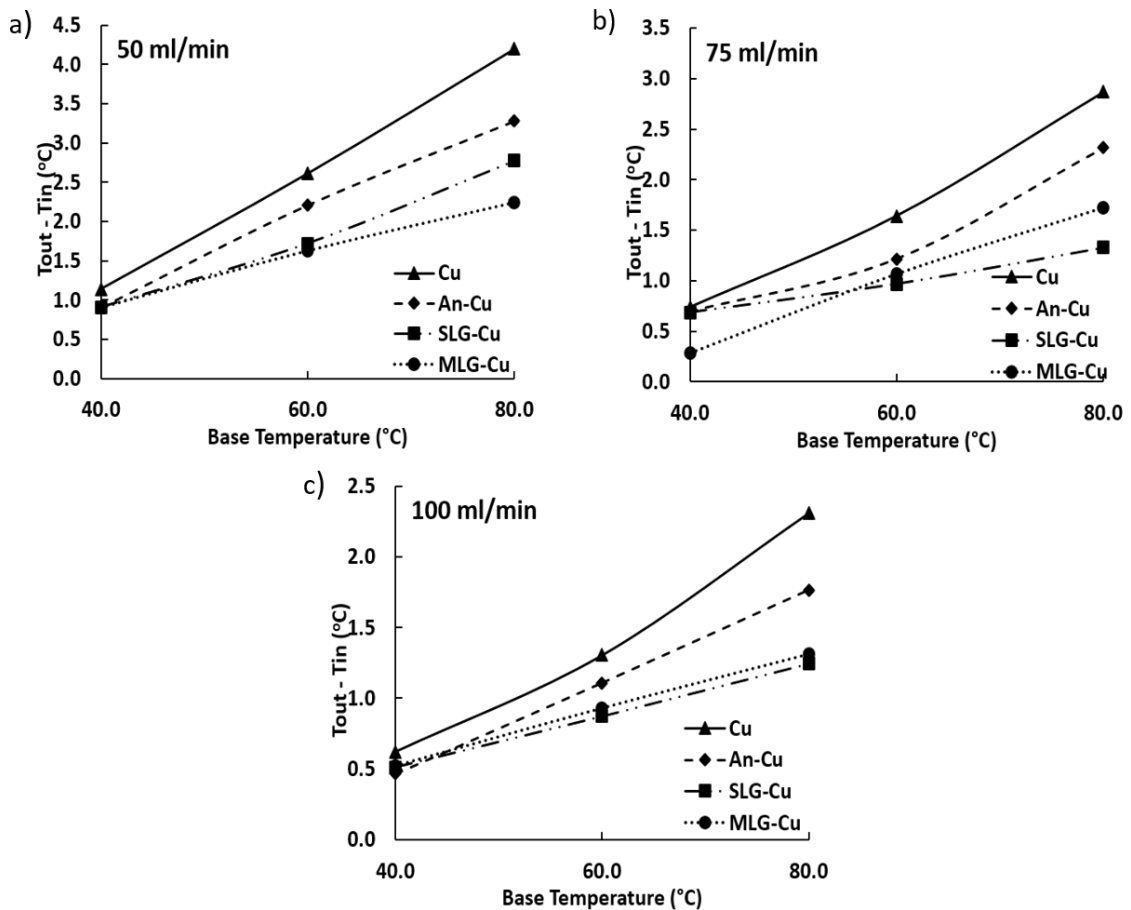
Figure 3.16. The temperature differences between water outlet and inlet (Tout-Tin) at different base temperature with different flow rates a) 50 ml/min, b) 75 ml/min and, c) 100 ml/min.

Figure 3.16 shows that coated samples transfer heat to the water in a limited manner. Also, for all flow rate and temperature, the temperature difference between water inlet and outlet decreases when the flow rate was raised. This is because the heat is removed quickly from the material.

3.3. Conclusion

In this chapter we have presented experimental investigations of thermal performance of graphene coated copper. Thermal performance of pure Cu, An-Cu, SLG-Cu, and MLG-Cu foil tested under different volume flow rate and based temperature.

Results show that, the heat fluxes get a higher value when the based temperature and volume flow rates increase. Un-coated samples transfer heat to the water directly

compared to coated ones. Thus, it is required higher heat flux to keep them near the based temperature compared coated ones. Another outcome is that, graphene coated sample have lower temperature rising compared to un-coated ones. This is because it can be explained that the samples that are coated with graphene are removed heat quickly from themselves without giving it to the water.

Graphene can improve the thermal properties of the material according to the heat conduction direction. As is this study, heat flux gives the samples in through plane direction so it was observed that graphene-coated samples couldn't transfer heat to the water good compare to un-coated ones.

CHAPTER 4

CONCLUSION AND FUTURE WORK

In the scope of the thesis, thermal performance of Cu, An-Cu, SLG-Cu and MLG-Cu was investigated numerically and experimentally. First part of the study about thermal conductivity calculation using MD simulation method. C++ programming language is used for create the model structure and algorithms for MD simulation. Thermal conductivity of copper, different number of graphene layers and these graphene layers were coated on copper in different length, width, height and temperature were investigated. Results show that graphene coating improves the thermal conductivity of copper.It was seen that SLG has the highest thermal conductivity compared to the other models. In addition, among the graphene-coated copper models, MLG-Cu has the highest thermal conductivity.

In the second part, the thermal performance of pure copper, annealed copper, a layer of graphene-coated copper, and multi-layer graphene-coated copper was studied by an experimental setup at three different temperatures and volume flow rates. It was observed that graphene-coated samples couldn't transfer heat to the water good compare to un-coated ones because of graphene heat conduction direction.

As a future work, as a numerical study defected graphene structure and coating on copper will be investigated. Also, in this study in-plane direction thermal conductivity is studied, for the future study through-plane direction thermal conductivity will be examined for heat pass through from metal to graphene. In addition, it was planning that experimental setup will be developed and thermal properties of different materials will be examined.

REFERENCES

Alder, B. J. and T. E. Wainwright (1959). Studies in molecular dynamics. i. general method. *The Journal of Chemical Physics 31*(2), 459–466.

Ashcroft, N. W. and N. D. Mermin (1976). Solid state physics.

Balandin, A. A. (2011, aug). Thermal properties of graphene and nanostructured carbon materials. *Nature Materials 10*(8), 569–581.

Balandin, A. A., S. Ghosh, W. Bao, I. Calizo, D. Teweldebrhan, F. Miao, and C. N. Lau (2008). Superior thermal conductivity of single-layer graphene. *Nano letters 8*(3), 902–907.

Brenner, D. W., O. A. Shenderova, J. A. Harrison, S. J. Stuart, B. Ni, and S. B. Sinnott (2002). A second-generation reactive empirical bond order (rebo) potential energy expression for hydrocarbons. *Journal of Physics: Condensed Matter 14*(4), 783.

Cai, W., A. L. Moore, Y. Zhu, X. Li, S. Chen, L. Shi, and R. S. Ruoff (2010). Thermal transport in suspended and supported monolayer graphene grown by chemical vapor deposition. *Nano letters 10*(5), 1645–1651.

Cao, H.-Y., Z.-X. Guo, H. Xiang, and X.-G. Gong (2012). Layer and size dependence of thermal conductivity in multilayer graphene nanoribbons. *Physics Letters A 376*(4), 525–528.

Chen, L. and S. Kumar (2012). Thermal transport in graphene supported on copper. *Journal of Applied Physics 112*(4), 043502.

Frenkel, D. and B. Smit (2001). *Understanding molecular simulation: from algorithms to applications*, Volume 1. Elsevier.

Gao, Z., Y. Zhang, Y. Fu, M. Yuen, and J. Liu (2013). Graphene heat spreader for thermal management of hot spots. *Proceedings - Electronic Components and Technology Conference 61*, 2075–2078.

Ghosh, d., I. Calizo, D. Teweldebrhan, E. P. Pokatilov, D. L. Nika, A. A. Balandin, W. Bao, F. Miao, and C. N. Lau (2008). Extremely high thermal conductivity of graphene: Prospects for thermal management applications in nanoelectronic circuits. *Applied Physics Letters 92*(15), 151911.

Goli, P., H. Ning, X. Li, C. Y. Lu, K. S. Novoselov, and A. A. Balandin (2014, mar). Thermal properties of graphene-copper-graphene heterogeneous films. *Nano Letters 14*(3), 1497–1503.

Guo, Z., D. Zhang, and X.-G. Gong (2009). Thermal conductivity of graphene nanoribbons. *Applied physics letters 95*(16), 163103.

Hong, Y., L. Li, X. C. Zeng, and J. Zhang (2015). Tuning thermal contact conductance at graphene–copper interface via surface nanoengineering. *Nanoscale 7*(14), 6286–6294.

Hoover, W. G. (1985, mar). Canonical dynamics: Equilibrium phase-space distributions. *Physical Review A 31*(3), 1695–1697.

Hsieh, C. T., Y. F. Chen, C. E. Lee, Y. M. Chiang, K. Y. Hsieh, and H. S. Wu (2017). Heat transport enhancement of heat sinks using Cu-coated graphene composites. *Materials Chemistry and Physics 197*, 105–112.

Hu, J., Y. Ji, Y. Shi, F. Hui, H. Duan, and M. Lanza (2014). A review on the use of graphene as a protective coating against corrosion. *Ann. J. Mater. Sci. Eng 1*, 16.

Jagannadham, K. (2012). Thermal conductivity of copper-graphene composite films synthesized by electrochemical deposition with exfoliated graphene platelets. *Metallurgical and Materials Transactions B 43*(2), 316–324.

Kang, C. G., S. K. Lim, S. Lee, S. K. Lee, C. Cho, Y. G. Lee, H. J. Hwang, Y. Kim, H. J. Choi, S. H. Choe, M.-H. Ham, and B. H. Lee (2013, mar). Effects of multi-layer graphene capping on Cu interconnects. *Nanotechnology 24*(11), 115707.

Kang, H., Y. Zhang, and M. Yang (2011). Molecular dynamics simulation of thermal conductivity of cu–ar nanofluid using eam potential for cu–cu interactions. *Applied Physics A 103*(4), 1001.

Kang, J., H. Kim, K. S. Kim, S.-K. Lee, S. Bae, J.-H. Ahn, Y.-J. Kim, J.-B. Choi, and B. H. Hong (2011). High-performance graphene-based transparent flexible heaters. *Nano letters 11*(12), 5154–5158.

Lebedeva, I. V., A. A. Knizhnik, A. M. Popov, Y. E. Lozovik, and B. V. Potapkin (2011). Interlayer interaction and relative vibrations of bilayer graphene. *Physical Chemistry Chemical Physics 13*(13), 5687–5695.

Lee, C., X. Wei, J. W. Kysar, and J. Hone (2008). Measurement of the elastic properties and intrinsic strength of monolayer graphene. *science 321*(5887), 385–388.

Lee, S., J. Hong, J. H. Koo, H. Lee, S. Lee, T. Choi, H. Jung, B. Koo, J. Park, H. Kim, Y. W. Kim, and T. Lee (2013). Synthesis of few-layered graphene nanoballs with copper cores using solid carbon source. *ACS Applied Materials and Interfaces 5*(7), 2432–2437.

Li, X., W. Cai, J. An, S. Kim, J. Nah, D. Yang, R. Piner, A. Velamakanni, I. Jung, E. Tutuc, S. K. Banerjee, L. Colombo, and R. S. Ruoff (2009). Large-area synthesis of high-quality and uniform graphene films on copper foils. *Science 324*(5932), 1312–1314.

Li, X., Y. Zhu, W. Cai, M. Borysiak, B. Han, D. Chen, R. D. Piner, L. Colombo, and R. S. Ruoff (2009). 34.Transfer of Large-Area Graphene Films for High-Performance Transparent Conductive Electrodes. *Nano Lett. 9*(12), 4359–4363.

Lindsay, L. and D. Broido (2010). Optimized tersoff and brenner empirical potential parameters for lattice dynamics and phonon thermal transport in carbon nanotubes and graphene. *Physical Review B 81*(20), 205441.

Mehta, R., S. Chugh, and Z. Chen (2015, mar). Enhanced Electrical and Thermal Conduction in Graphene-Encapsulated Copper Nanowires. *Nano Letters 15*(3), 2024–2030.

Momenzadeh, L., A. V. Evteev, E. V. Levchenko, I. V. Belova, G. E. Murch, and Y. H. Sohn (2013). Phonon Thermal Conductivity of F.C.C. Cu by Molecular Dynamics Simulation. *Defect and Diffusion Forum 336*(Md), 169–184.

Mortazavi, B. and S. Ahzi (2012, aug). Molecular dynamics study on the thermal conductivity and mechanical properties of boron doped graphene. *Solid State Communications 152*(15), 1503–1507.

Mortazavi, B., A. Rajabpour, S. Ahzi, and A. Hadizadeh (2012). Non-Equilibrium Molecular Dynamics Study on the Thermal and Mechanical Properties of Graphene. *I.R. Iran*, 12–14.

Nika, D. and A. A. Balandin (2016). *Thermal Transport in Low Dimensions*, Volume 921.

Novoselov, K. S. and A. Geim (2007). The rise of graphene. *Nat. Mater 6*(3), 183–191.

Novoselov, K. S., A. K. Geim, S. V. Morozov, D. Jiang, Y. Zhang, S. V. Dubonos, I. V. Grigorieva, and A. A. Firsov (2004). Electric field effect in atomically thin carbon films. *science 306*(5696), 666–669.

Pop, E., V. Varshney, and A. K. Roy (2012). Thermal properties of graphene: Fundamentals and applications. *MRS Bulletin 37*(12), 1273–1281.

Rahman, A. (1964). Correlations in the motion of atoms in liquid argon. *Physical Review 136*(2A), A405.

Salihoglu, O., H. B. Uzlu, O. Yakar, S. Aas, O. Balci, N. Kakenov, S. Balci, S. Olcum, S. Süzer, and C. Kocabas (2018, jul). Graphene-Based Adaptive Thermal Camouflage. *Nano Letters 18*(7), 4541–4548.

Sharma, S., P. Kumar, and R. Chandra (2017). Mechanical and thermal properties of graphene–carbon nanotube-reinforced metal matrix composites: A molecular dynamics study. *Journal of Composite Materials 51*(23), 3299–3313.

Shenoy, S. (2012). Thermal conductances of aligned structures and thin films with embedded carbon nanotubes.

Si, C., X.-D. Wang, Z. Fan, Z.-H. Feng, and B.-Y. Cao (2017). Impacts of potential models on calculating the thermal conductivity of graphene using non-equilibrium molecular dynamics simulations. *International Journal of Heat and Mass Transfer 107*, 450–460.

Sidorenkov, A. V., S. V. Kolesnikov, and A. M. Saletsky (2016). Molecular dynamics simulation of graphene on cu (111) with different lennard-jones parameters. *The European Physical Journal B 89*(10), 220.

Stillinger, F. H. and A. Rahman (1974). Improved simulation of liquid water by molecular dynamics. *The Journal of Chemical Physics 60*(4), 1545–1557.

Stuart, S. J., A. B. Tutein, and J. A. Harrison (2000). A reactive potential for hydrocarbons with intermolecular interactions. *The Journal of chemical physics 112*(14), 6472–6486.

Sutton, A. and J. Chen (1990). Long-range finnis–sinclair potentials. *Philosophical Magazine Letters 61*(3), 139–146.

Tersoff, J. (1988). New empirical approach for the structure and energy of covalent systems. *Physical Review B 37*(12), 6991.

Usha Kiran, N., S. Dey, B. Singh, and L. Besra (2017). Graphene coating on copper by electrophoretic deposition for corrosion prevention. *Coatings 7*(12), 214.

Vera, J. G. (2014, nov). Temperature and Heat Flux Dependence of Thermal Resistance of Water/Metal Nanoparticle Interfaces.

Wei, Z., Z. Ni, K. Bi, M. Chen, and Y. Chen (2011). In-plane lattice thermal conductivities of multilayer graphene films. *Carbon 49*(8), 2653–2658.

Wejrzanowski, T., M. Grybczuk, M. Chmielewski, K. Pietrzak, K. J. Kurzydlowski, and A. Strojny-Nedza (2016). Thermal conductivity of metal-graphene composites. *Materials and Design*.

Wejrzanowski, T., M. Grybczuk, M. Wasiluk, and K. J. Kurzydlowski (2015). Heat transfer through metal-graphene interfaces. *AIP Advances 5*(7), 077142.

Yin, L., T. Nan, P. He, Z. Chen, L. Yang, and J. Zhang (2017, jan). Thermal Performance Enhancement of Light Emitting Diode Device with Multilayer-Graphene Transferred to the Substrate Surface. *ECS Journal of Solid State Science and Technology 6*(1), R35–R39.

Yu, C. and G. Zhang (2013). Impacts of length and geometry deformation on thermal conductivity of graphene nanoribbons. *Journal of Applied Physics 113*(4), 044306.

Zhu, F., Y. Kan, K. Tang, and S. Liu (2017). Investigation of Thermal Properties of Ni-Coated Graphene Nanoribbons Based on Molecular Dynamics Methods. *Journal of Electronic Materials 46*(8), 4733–4739.